Single cell trajectory modeling identifies a primitive trophoblast state defined by BCAM enrichment

Matthew Shannon[1,2], Jennet Baltayeva[1,2], Barbara Castellana[1,2], Jasmin Wächter[1,2], Samantha Yoon[1,3], Jenna Treissman[1,2], Hoa Le[1,3], Alexander G. Beristain[1,2]

[1] The British Columbia Children's Hospital Research Institute, Vancouver, Canada.
[2] Department of Obstetrics & Gynecology, The University of British Columbia, Vancouver, Canada.
[3] Department of Surgery, The University of British Columbia, Vancouver, Canada.

To whom correspondence should be addressed: Alexander G. Beristain, The British Columbia Children's Hospital Research Institute, The University of British Columbia, Vancouver, British Columbia, Canada. V5Z 4H4. Tel: (604) 875-3573; E-mail: aberista@mail.ubc.ca

Keywords: Placenta, trophoblast, single cell RNA-sequencing, extravillous trophoblast, villous cytotrophoblast, cell differentiation,

Summary Statement: A trophoblast progenitor niche enriched in BCAM shows complex cell trajectory dynamics and gene signaling pathways

Abbreviations

CTB: Cytotrophoblast
DCT: Distal column trophoblast
DGE: Differential gene expression
EVT: Extravillous trophoblast
FDR: False discovery rate
GO: Gene ontology
HLA-G: Human leukocyte antigen G
Hr: Hour
RT: Room Temperature
IF: Immunofluorescence
scRNA-seq: single cell RNA sequencing
SCT: Syncytiotrophoblast
UMAP: Uniform manifold approximation and projection

ABSTRACT

The establishment and function of the human placenta is dependent on specialized cells called trophoblasts. Progenitor cytotrophoblasts (CTBs) differentiate along one of two cellular trajectories: the villous or extravillous pathways. CTBs committed to the villous pathway fuse with neighboring CTBs forming the outer multinucleated syncytiotrophoblast layer (SCT), while CTBs committed to the extravillous pathway develop into multi-layered cell columns that anchor the placenta to uterine tissue. At distal column sites, column CTBs differentiate into invasive extravillous trophoblasts (EVT) that facilitate uterine remodeling of spiral arteries and modulate the maternal immune response to fetal antigen. Unfortunately, little is known about the cellular and molecular processes controlling human trophoblast stem cell maintenance and differentiation into these critical trophoblast sub-lineages. To address this, our laboratory established a single cell RNA sequencing (scRNA-seq) dataset from first trimester placentas to identify molecular programs and cell states important in trophoblast progenitor establishment, renewal, and differentiation. Using this dataset, eight distinct trophoblast states were identified, representing progenitor cytotrophoblasts, intermediate column CTBs, syncytiotrophoblast progenitors, and terminally differentiated EVT. Lineage trajectory analysis identified a CTB origin that was reproduced in human trophoblast stem cell organoids. Heightened expression of basal cell adhesion molecule (*BCAM*) defined this primitive state, where CTBs selected for high levels of surface BCAM expression generated larger clonally-derived organoids than did CTB counterparts expressing lower levels of BCAM. Together, this work resolves complex gene networks within human trophoblast progenitor cells, and identifies BCAM as marker that defines an up-stream progenitor origin.

70 **INTRODUCTION**

71 The placenta is a blastocyst-derived tissue that shares the genetic identity of the developing
72 fetus. Derived from cells of the trophectoderm and extraembryonic mesoderm, the human placenta
73 matures into a functional organ by 10-12 weeks' gestation (GA)[1-3]. Through its direct interaction with
74 maternal uterine epithelial, stromal, and immune cells, the placenta coordinates the establishment of the
75 maternal-fetal-interface and serves as a critical barrier important for nutrient-waste exchange between
76 maternal and fetal circulations. Trophectoderm-derived trophoblasts perform many functions of the
77 placenta. These include, but are not limited to the facilitation of nutrient and oxygen transfer between
78 mother and fetus[4], the modulation of the maternal immune response towards the semi-allogeneic fetus
79 and placenta[5,6], and the production of hormones (i.e. chorionic gonadotropin, progesterone, placental
80 lactogen) and other factors required for pregnancy[7].

81 Of all eutherian mammals, the human placenta is the most invasive[3]. Though humans and
82 rodents both share a haemochorial arrangement of trophoblast and uterine tissue, control of uterine
83 surface epithelial and stromal erosion, as well as artery remodeling by trophoblasts during blastocyst
84 implantation and early placental establishment is far more extensive in humans than in rodents[8].
85 Importantly, key regulators of trophoblast lineage specification in rodents (i.e. *Cdx2*, *Eomes*, *Esrrb*, and
86 *Sox2*) do not appear to play essential (or identical in the case of *Cdx2*) roles in human trophoblasts[9].
87 These important differences in human trophoblast biology underlie the need to use human placentas
88 and cell systems for generating fundamental knowledge central to human trophoblast and placental
89 development. While recent advances in regenerative trophoblast culture systems have created the
90 necessary tools required for in-depth cellular and molecular understandings central to trophoblast
91 differentiation[10-12], to date, few studies have used these platforms to examine at high resolution
92 trophoblast progenitor and/or stem cell dynamics.

93 In humans, two major trophoblast differentiation pathways – villous and extravillous – give rise

to all trophoblasts in the fetal-maternal interface (Figure 1A). In the villous pathway, progenitor cytotrophoblasts (CTBs) fuse with neighboring CTBs to replenish or generate new syncytiotrophoblast (SCT), a multinucleated outer layer of the placenta that is the site of transport of most substances across the placenta, and is also the placenta's major metabolic and endocrine engine. Cells committed to differentiate along the extravillous pathway are predicted to originate from CTB progenitors proximal to anchoring villi[9], though populations of villous CTB may already be programmed towards extravillous differentiation or may alternatively harbor a level of bi-potency[2,13]. Nonetheless, progenitors devoted to this pathway give rise to extravillous trophoblasts (EVTs) that anchor the placenta to the uterine wall (i.e. proximal and distal column CTB) and these cells adopt invasive characteristics hallmarked by interstitial and endovascular EVT subsets that facilitate uterine tissue and artery remodeling, and interact with and modulate maternal immune cell activity[14-16]. Defects in trophoblast differentiation along either pathway associate with impaired placental function that may contribute to, or drive, the development of aberrant conditions of pregnancy[17].

In this study, we integrate an in-house first trimester placenta single cell RNA-sequencing (scRNA-seq) dataset (7 unique placentas) with a publicly available first trimester placenta/decidual scRNA-seq dataset consisting of 4 additional samples[18]. Using this data, we investigate trophoblast heterogeneity across the first trimester and identify a CTB origin state that likely represents a trophoblast stem cell/progenitor population. Within this upstream progenitor state, we show elevated expression of the gene *Basal Cell Adhesion Molecule* (*BCAM*), where isolation and culture of BCAM^{hi} CTBs result in robust organoid establishment and growth. Together, this work reaffirms prior findings related to CTB biology, maintenance, and renewal, and further identifies new gene pathways underlying distinct CTB progenitor/stem states upstream of SCT and EVT sub-lineage commitment that are central to placental development.

118 **RESULTS**

119 **Single cell transcriptomics resolves trophoblast heterogeneity and cell state dynamics**

120 Single-cell transcriptomic analysis enables the identification of novel cell types and cell states
121 in a systematic and quantitative manner. Here, we applied the 10X Genomics Chromium platform to
122 sequence the healthy human placental transcriptome at single cell resolution (n=7 placentas), and
123 merged this data with publicly available single-cell transcriptomic profiles of healthy human maternal-
124 fetal interface tissues (n=4 placentas, n=4 deciduas) (Figure 1B). To examine developmental
125 differences, we grouped individual samples into early (6-7 weeks') and late (9-12 weeks') gestational
126 age (GA) ranges. Clinical characteristics and sequencing metrics from each patient and sample are
127 summarized in Supplemental Tables 1 and 2. 50,790 cells remained after quality control and data pre-
128 processing (Supplemental Figure 1A-C). Principal component (PC) analysis validated data integration
129 between our placental data and the maternal-placental interface data collected from ArrayExpress[18]
130 with separation of cells explained by tissue type, not data source (Supplemental Figure 1D). These cells
131 were clustered into 14 cell types and 31 distinct cell states by transcriptomic similarity (Supplemental
132 Figure 1E). The influence of fetal gestational age on placental and decidual cell composition was
133 compared, where late first trimester samples showed greater uterine cell coverage than early samples
134 (Supplemental Figure 1F). All clusters were identified by comparing gene expression profiles
135 (Supplemental Figure 1G), and cell cycle phase proportions per cluster informed the level of
136 proliferation in each cell state within the first trimester (Supplemental Figure 1H). Decidual cells were
137 identified by vimentin expression and decidual immune cells were specifically identified by *PTPRC*
138 transcripts that encode the leukocyte CD45 antigen (Supplemental Figure 1I). Additional markers were
139 used to identify endothelial, stromal, and fibroblastic cell compartments of the maternal fetal interface,
140 defining the heterogeneous landscape and dynamic nature of these cells (Supplemental Figure 1I).

141 For trophoblast identification, cells expressing combinations of trophoblast-related transcripts

142 (i.e. *KRT7*, *EGFR*, *TEAD4*, *TP63*, *TFAP2A*, *TFAP2C*, *GATA2*, *GATA3*, *HLA-G*, *ERVFRD-1*), and
143 lacking mesenchymal- and immune-related transcripts (i.e. *VIM*, *WARS*, *PTPRC*, *DCN*, *CD34*, *CD14*,
144 *CD86*, *CD163*, *NKG7*, *KLRD1*, *HLA-DPA1*, *HLA-DPB1*, *HLA-DRA*, *HLA-DRB1*, *HLA-DRB5*, and
145 *HLA-DQA1*), were subset for further analysis (Supplemental Figure 1G, 1J). Eight distinct trophoblast
146 clusters from 7,798 cells were resolved (Figure 1C). Within these 8 clusters, we identified four CTB
147 states (CTB1-4; *EGFR*$^+$, *ELF5*$^+$), a CTB state expressing the SCT-related genes that we termed
148 progenitor syncytiotrophoblast (SCTp; *ERVFRD-1*$^+$, *CGB*$^+$), two column trophoblast states (cCTB1-2;
149 NOTCH1$^+$, ITGA5$^+$), and a state specific to EVT (EVT; *HLA-G*$^+$, *ITGA1*$^+$) (Figure 1C, 1D;
150 Supplemental Table 3). Moreover, CTB1-4 showed varying degrees of enrichment for genes associated
151 with trophoblast progenitor/stem states (i.e. *CDX2, TP63*, *ELF5*, *TEAD4*), where CTB2 and CTB3
152 showed the greatest enrichment for progenitor genes (Figure 1D).

153 Column trophoblasts are precursors to EVT, where cells situated within proximal and distal
154 sites of anchoring columns can be molecularly distinguished by expression of distinct NOTCH and
155 integrin genes[19,20]. To this end, cCTB2 expresses high levels of *NOTCH1*, *SOX9,* and *ITGA2*, the latter
156 of which defines a distinct EVT progenitor population[13] and therefore likely represents a proximal
157 column EVT progenitor (Figure 1D). Compared to cCTB2, cells within the cCTB1 state showed higher
158 levels of *ITGA5*, *NOTCH2*, and *HLA-G*, indicating that this state is developmentally downstream of
159 cCTB2 and cells within this state likely reside within central and distal regions of anchoring columns[21]
160 (Figure 1D). Stratifying cells by phases of the cell cycle showed that cCTB1 column cells are
161 predominately in G2, M, and S phases, while cCTB2 column cells are not actively cycling (Figure 1E).
162 As expected, terminally differentiated EVT and SCTp states are largely non-cycling G1 cells, as are
163 progenitor CTB1-3 states (Figure 1E). This was in contrast to CTB4, where the vast majority of cells
164 are actively cycling and express hallmark genes linked to proliferation (i.e. *MKI67*, *CCNA2*) (Figure
165 1D-F). Importantly, these distinct trophoblast states largely align with recent single cell transcriptomic

166 characterizations of cells from first trimester pregnancies[18,22,23].

167 Having defined eight trophoblast types/states within first trimester placental villi, we next
168 examined their stability across the first trimester developmental period. Relative steady-state
169 frequencies in CTB1 and CTB3 states were observed in placentas from 6-7 weeks' and 9-12 weeks'
170 GA, whereas more dynamic changes were seen in other states (Figure 1G). The proportion of cells
171 comprising the proliferative CTB4 state decreased slightly from the early (18%) to late (11%) first
172 trimester (Figure 1G). Moderate decreases in frequency were also seen in cells within column (cCTB1,
173 cCTB2), EVT, and SCTp states (Figure 1G). This was in mark contrast to CTB2, which showed a ~3-
174 fold increase from 8% to 29% (Figure 1G). Together, these findings define unique states of trophoblast
175 heterogeneity in the early and late first trimester developmental window, a developmental period
176 correlating with an onset in maternal blood perfusion within the intervillous space around 10 weeks'
177 GA, and a significant expansion/branching of floating placental villi.

178

179 **Defining known and novel gene programs in CTB progenitor maintenance and differentiation**

180 With the recent development of regenerative human trophoblast models that better facilitate the
181 study of progenitor CTB differentiation into SCT and EVT, significant strides have been made in our
182 understanding of key pathways underlying CTB establishment, maintenance, and the initial molecular
183 programs driving CTB differentiation[10-12,24,25]. For example, WNT, HIPPO, and EGFR signaling are
184 essential in human trophoblast stem cell establishment[10-12], and impairments in trophoblast stem cell
185 regeneration in the context of YAP-TEAD4 complex perturbation[24,25] underscore the necessity of these
186 pathways in placental development. To examine how previously described pathways critical to CTB
187 development are altered during differentiation, we applied a simple branched pseudotime trajectory
188 analysis (using Monocle2) to order cells and states in pseudotime (Supplemental Figure 2A, 2B). We

189 focused on the transitions occurring between trophoblast cell type, and more specifically cell state, with
190 increased pseudotime maturation along either of the defined villous or extravillous trajectories
191 (Supplemental Figure 2B). While simple branched pseudotime ordering did not resolve a
192 developmental lineage within the four CTB states, a predicted cell state/type origin was identified
193 comprising cells within CTB1-4, and pseudotime ordering did delineate a transition from cCTB2 into
194 cCTB1 which further progress towards EVT (Supplemental Figure 2B). Monocle2 ordering also
195 highlighted the transition from CTB to SCTp; these findings are in line with recent pseudotime
196 ordering characterization of trophoblasts showing a defined origin and two differentiation trajectory
197 branches[18].

198 Aligning WNT, HIPPO, and EGFR pathway genes to the Monocle2 pseudotime trajectory
199 showed distinct patterns of gene expression in cells with proximity to the predicted origin, within
200 intermediate states along both the SCT and EVT differentiation pathways, as well as in terminally
201 differentiated SCTp and EVT states (Supplemental Figure 2C, 2D). In agreement with previous studies,
202 Dickkopft-1 (*DKK1*; an inhibitor of Wnt signaling), leucine-rich repeat-containing G-protein coupled
203 receptor 6 (*LGR6*; a Wnt receptor), the Wnt ligand genes *WNT5B* and *WNT5A*, the HIPPO signaling
204 genes transcriptional enhancer factor TEF-3 (*TEAD4*) and protein salvador homolog 1 (*SAV1*), and the
205 EGFR ligand betacellulin (*BTC*) are enriched within CTB cell states aligning to or proximal to the
206 predicated origin (Supplemental Figure 2C, 2D). As trophoblasts progress along the EVT pathway,
207 expression levels of specific Wnt-related genes (i.e. *AXIN2*, *WNT11*, *WNT9A*, *FZD4*) and the EGFR
208 ligand *AREG* transiently increase within intermediate cCTB states (Supplemental Figure 2C, 2D).
209 Nearing terminal EVT differentiation, the Wnt-ligand *WNT10B* markedly increases, as do specific
210 HIPPO-related transcription factors (*TEAD2*, *TEAD1*), and modulators (*FAT1*, *FAT2*, *WWTR1*), and the
211 EGFR receptor *ERBB2* (Supplemental Figure 2C, 2D). Along the villous trajectory, SCT progenitors
212 up-regulate the Wnt receptor *FZD1* and multiple Wnt ligands (*WNT2*, *WNT2B*, *WNT3A*, *WNT7A*), as

213 well as the HIPPO pathway transcription factor TEAD3 and the EGFR's *ERBB3* and *ERBB4*
214 (Supplemental Figure 2C, 2D). Together, lineage trajectory modeling and alignment of key
215 genes/pathways known to be important in CTB regeneration and differentiation provides a
216 comprehensive landscape of distinct effectors and regulators putatively controlling trophoblast
217 development in early pregnancy.

218 To resolve the genetic similarities and differences between distinct CTB states, all four CTB
219 states were subset for targeted transcriptomic analyses (Figure 2A). Next, we compared CTB1-4 using
220 the top 10 unique genes expressed in each state (Figure 2B). This approach characterized CTB1 as a
221 translationally active cell state, CTB2 as a cell state made up of more classically defined CTBs (i.e.
222 expressing *SPINT1*), CTB3 as a metabolically active state defined by mitochondrial gene enrichment,
223 and CTB4 as a proliferative state (Figure 2B). The similarities in gene expression across all four CTB
224 states revealed 944 genes upregulated within all CTBs (compared to more differentiated trophoblast
225 states), including the known CTB markers *TP63*, *EGFR*, and *TEAD4* (Figure 2D; Supplemental Table
226 4). Specific to each CTB state, we found upregulation of *PGF* in CTB1, upregulation of the
227 extracellular laminin gene *LAMC2* and the transcription factor *HOXB2* in CTB2, upregulation of
228 *GATA2*, *FZD3*, and *AXIN2* in CTB3, and upregulation of *TFAP4* and *TFAP2B* in CTB4 (Supplemental
229 Table 4). Gene ontology terms enriched from those genes uniquely upregulated in each state revealed
230 that CTB1 is involved in general metabolic processes (Figure 2E), CTB2 is involved in cell stemness
231 and general responses to hypoxia (Figure 2E), CTB3 has terms describing the suppression of
232 mitochondrial activity and promoting cell anabolism (Figure 2E), and CTB4, is involved in cell cycle
233 progression and chromosome organization/segregation (Figure 2E). Finally, *cis*-regulatory sequence
234 analysis of the enriched genes per CTB state revealed a list of 62 transcription factors (TFs) that may
235 act as CTB-specific regulators (Figure 2F). Included in this list are TFs known to be important in CTB
236 biology like *TEAD4* and *TFAP2A*[25]. Interestingly, TFs such as transcriptional regulator KAISO

237 (*ZBTB33*) involved the negative regulation of the WNT pathway[26] shows enrichment in CTB3. These
238 findings highlight the cellular and molecular complexity within the CTB compartment of the placenta,
239 and identify possible transcriptional regulators important in controlling the maintenance of progenitor
240 CTBs as well as regulating the possible transition between unique CTB states.

241

242 **Single cell trajectory modeling identifies a CTB origin**

243 RNA velocity, the time derivative of the gene expression state, can be used to predict the future
244 transcriptional state of a cell. RNA velocity analysis in combination with single-cell trajectory analyses
245 provides us with insights into the transcriptional dynamics of developing cells and enables high-
246 resolution lineage pathway ordering. By applying scVelo to our dataset to further refine progenitor and
247 cell end-point relationships, we identified CTB2 as a first trimester placental trophoblast progenitor
248 origin from which all other trophoblasts derive (Figure 3A). We identified two paths extending from
249 this origin towards the EVT state and one path developing from the origin towards the SCTp state. As
250 well, we found an additional differentiation trajectory, extending from CTB2 into CTB3, representing
251 possible CTB progenitor reserves or progenitor states in transition.

252 To more completely understand the developmental steps involved in CTB differentiation, we
253 applied complex pseudotime ordering using Monocle3. Similar to RNA velocity, CTB2 was identified
254 as the CTB origin showing increased complexity as CTBs progress along one of two trajectories that
255 lead to either EVT or SCT end-point states (Supplemental Figure 3A, 3B). Specifically, complex
256 pseudotime ordering revealed a looped trajectory within CTB2 that exits towards CTB3, SCTp, and
257 EVT states (Supplemental Figure 3C). We compared these refined trajectories with expression patterns
258 of known CTB progenitor/stem cell genes. Predominant expression of *ELF5*, *YAP1*, and *ITGA6* was
259 observed in CTB3, while expression of CTB stem cell transcription factor *CDX2* showed predominant

260 expression within the CTB2 state (Figure 3B). Because CTB2 and CTB3 shared expression of multiple
261 trophoblast progenitor genes, we examined genes both shared and unique to these states (Figure 3C).
262 Twenty-five genes were shown to overlap between CTB2 and CTB3, including the genes *EGFR, IGF2,*
263 and *FBLN1* (Figure 3C). The CTB3 progenitor state expressed 274 unique genes, and of these genes,
264 many associate with trophoblast stem cell and regenerative properties (i.e. *YAP1, TP63*), Wnt signaling
265 (*LRP5*), and cell-matrix interactions (*MMP14, MMP15, ITGA6, LAMA5, LAMB1*) (Figure 3C). The
266 predicted CTB2 origin expressed 269 unique genes, including the Wnt ligand, *WNT7A*, the laminin
267 receptor basal cell adhesion molecule (*BCAM*), and the transcriptional modulators *TFAP2A* and
268 *CITED2* (Figure 3C). The expression patterns of select genes in these CTB states over pseudotime
269 support scVelo and Monocle3 trajectory ordering suggesting that CTB2 is upstream of CTB3 (Figure
270 3D; Supplemental Figure 3C). Focusing specifically on the CTB2 origin state, we identified the
271 enrichment of *BCAM*, a gene encoding a laminin cell surface receptor (Figure 3E). Also enriched
272 within this primitive CTB2 state were the genes *SOD3*, *GPC3*, *EFEMP1*, *EPN3*, and *C10orf54* (Figure
273 3E). Cumulatively, we have identified a primitive CTB state within the first trimester placenta that
274 shows molecular features of a putative CTB stem cell population possessing a unique gene expression
275 profile that includes the early stem marker *CDX2* and the cell surface glycoprotein *BCAM*.

276

277 **Trophoblast stem cells recapitulate scRNA-seq-informed CTB heterogeneity and hierarchy**

278 Recently described regenerative human trophoblast models provide an improved method for
279 modeling trophoblast differentiation *in vitro*[10]. Three-dimensional organoid-like cultures of human
280 trophoblast stem cell lines (hTSCs) have also been shown to reproduce molecular features underlying
281 CTB maintenance and differentiation[25]. To examine the reproducibility of trophoblast-intrinsic
282 differentiation programs defined by scRNA-seq analysis of *in vivo* placental specimens, we subjected

283 three hTSC lines to scRNA-seq analysis prior to and following EVT-directed differentiation.
284 Regenerative and EVT differentiating hTSC organoids (i.e. CT27, CT29, and CT30 CTB lines) were
285 cultured for 7 days in regenerative Wnt^+ (containing the Wnt potentiators R-spondin and CHIR99021)
286 and EVT-differentiating Wnt^- (lacking R-spondin and CHIR99021) media, respectively, prior to single
287 cell workflow. To confirm the intactness of our model system, a separate cohort of hTSC organoids
288 were cultured over 21 days in these media and differentiation was assessed by light microscopy, flow
289 cytometry, and qPCR analysis. hTSC-derived organoids cultured in regenerative media established
290 large spherical colonies characterized in part by elevated expression of the CTB progenitor genes
291 *TEAD4* and *ITGA6* (Figure 4A, 4C). Moreover, expression of surface MHC-I (HLA-A, -B, -C) by flow
292 cytometry did not detect these MHC-I ligands in undifferentiated cultures, (Figure 4B). Comparatively,
293 hTSC organoids cultured in EVT differentiating Wnt^- media showed characteristic cellular elongations
294 and extensions from the organoid body (Figure 4A), as well as a marked decrease in levels of *TEAD4*
295 mRNA (Figure 4C). As expected, both immature (*ITGA5*, *NOTCH1*) and mature (*NOTCH2*, *HLA-G*)
296 EVT marker genes, as well as HLA-C and HLA-G surface expression increased along the EVT
297 differentiation time-line (Figure 4B, 4C), indicating that the 3D organoid model to study CTB
298 regeneration and EVT differentiation is intact.

299 13,395 regenerative and 40,572 EVT-differentiated hTSC organoid cells were then used to
300 generate single cell cDNA libraries following the 10X Genomics Chromium workflow. Combining
301 single cell transcriptomic data from CT27, CT29, and CT30 hTSC organoids resolved 7 distinct cell
302 states based on global gene expression signatures; three CTB (CTB1-3), a pre-syncytiotrophoblast
303 (SCTp), a putative column/EVT progenitor (cCTB), and two EVT-like states (EVT1, EVT2) were
304 identified (Figure 4D). Hallmark gene markers of trophoblast-lineage (*TFAP2A, TFAP2C*), CTB
305 progenitors (*TEAD4, YAP1, TP63, ITGA6, ELF5*), syncytiotrophoblast (*ERVFRD-1, ERVV-1, SDC1*),
306 immature (*ITGA5, ITGA2, NOTCH1*) and mature EVT (*ITGA1, NOTCH2, HLA-G*), as well as gene

307 markers of proliferation (*MKI67, CCNA2*) are shown corresponding to individual cell states (Figure
308 4D). CTB1-3 shared great overlap in gene expression, though CTB1 distinctly expressed proliferative
309 genes that also co-expressed at high levels the progenitor genes *TEAD4*, *TP63*, and *ELF5* (Figure 4D).
310 While CTB2 and CTB3 also expressed progenitor genes, their levels were comparatively lower than
311 levels in CTB1 (Figure 4D). The putative column/EVT progenitor state cCTB uniquely expressed
312 *ITGA2*, *SOX9*, and the immature EVT marker *NOTCH1*; at the gene level, this unique state resembles
313 the EVT progenitor population described in Lee *et al*[13], though unlike that progenitor population, this
314 state did not express high levels of proliferative genes (Figure 4D). States resembling more terminally
315 differentiated cell types showed strong enrichment for syncytial-like genes (SCTp) and EVT-associated
316 genes, with EVT1 showing the highest expression of *HLA-G* and *NOTCH2* (Figure 4D).

317 When scRNA-seq data for hTSC-derived organoids are plotted individually, overall cell state
318 complexity diminishes from 7 unique states to 5 states (Figure 4E). When comparing the three hTSCs
319 with each other, notable variances in cell states are observed (Figure 4E). While clearly defined
320 endpoint states are evident, variances defined by gene expression in CTB and cCTB states suggest that
321 the hTSC lines harbor cell differentiation kinetics that are different from each other (Figure 4E).
322 Nonetheless, within each hTSC-derived organoid, a CTB origin was revealed by estimation of RNA
323 velocity that overlapped with CTB1 (Figure 4E). When this origin was compared across each hTSC
324 line by relative gene expression, we found consistent up-regulation of the trophoblast stem cell genes
325 *TP63*, *YAP1*, and *PAGE4* compared to other states. However, we did see differences in the expression
326 of the *ELF5* stem gene between hTSCs and individual states. Expression of *ELF5* localized to the
327 origin in the CT27 hTSC line, but not within the origins of the CT29 or CT30 hTSC lines (Figure 4E).
328 Similar differences were observed for the proliferative gene markers *MKI67* and *CCNA2*, with positive
329 expression occurring in the origins of CT27 and CT30, but not in the origins of CT29 (Figure 4E).
330 When averaged across all hTSC lines, however, we observed consistent expression of *ELF5*, *BCAM*,

331 *MKI67*, and *CNNA2* within the CTB origin (Figure 4D). Comparison of transcriptional signatures
332 between the scVelo-determined origins in *in vivo* trophoblasts from chorionic villi and hTSC-derived
333 organoids highlights that there is considerable overlap between the CTB2 & 3 (*in vivo*) and CTB1& 2
334 (*in vitro*) states (Figure 4F). Notably, we show *BCAM* to be one of the most highly expressed genes
335 within primitive states identified *in vivo* and in hTSC (Figure 4G, 4H). This suggests that BCAM may
336 be a novel CTB stem cell or progenitor marker.

337

338 **BCAM-enrichment confers increased CTB regenerative potential**

339 To our knowledge, BCAM localization within the human placenta has never been reported. To
340 this end, we probed early (6.3 week) and late (11.2 week) first trimester placental villi specimens with
341 BCAM antibody (Figure 5A). A specific and strong BCAM signal was observed in CTB of both
342 developmental time-points, and serial sections stained with keratin-7 (KRT7) and HLA-G showed that
343 BCAM was present within proximal column cells, though the intensity of the signal was less than in
344 CTB (Figure 5A). Serial sections of villi stained with KRT7 and hCG clearly showed that BCAM is
345 absent from the syncytiotrophoblast outer layer (Figure 5A). In hTSC-derived organoids cultured in
346 regenerative Wnt^+ media, BCAM signal was specific to the outer CTB layer and absent within the
347 hCG^+ syncytium (Figure 5B). Dual-labeling with BCAM and Ki67 antibody in CT29 hTSC-derived
348 organoids showed that $BCAM^+$ CTB and proximal column trophoblasts also stained positive for the
349 proliferation marker (Figure 5B). Flow cytometry, which enables a quantitative measure of BCAM cell
350 frequency, showed that in dissociated $EGFR^+$ CTB from CT29-derived organoids, ~90% of CTBs are
351 BCAM positive (Figure 5C).

352 To test the regenerative potential of BCAM-expressing cells, $BCAM^{hi}$ and $BCAM^{lo}$ CTBs (i.e.
353 $EGFR^+$ trophoblasts) were sorted from CT29 hTSC organoids and seeded as single cells at a density of

354 125 cells/μl within Matrigel domes and cultured over 11 days (Figure 5D). While the colony take-rate
355 did not differ between BCAM^{hi} and BCAM^{lo} CTB organoids (Supplemental Figure 4), BCAM^{hi}
356 organoid colony size appeared to be larger by day 7 of culture, with BCAM^{hi} colonies being
357 significantly larger than BCAM^{lo} colonies on days 9-11 in culture (Figure 5E). Notably, flow
358 cytometry assessment of endpoint day 11 BCAM^{hi} and BCAM^{lo} organoids showed that while BCAM^{hi}-
359 sorted cells retained frequencies of >90% BCAM high-expressing cells (Figure 5F), the frequency of
360 CTBs expressing BCAM in BCAM^{lo}-sorted cells was only marginally less, suggesting that the BCAM
361 phenotype is dynamic. Comparing differentially expressed genes between BCAM^{hi} and BCAM^{lo}
362 EGFR+ CTBs showed that BCAM^{hi} cells expressed higher levels of the paternally imprinted
363 transcription factors *PEG3* and *PEG10* involved in potentiating progression through the cell cycle and
364 stem cell renewal genes *EPCAM* and *HMGB3*[27] (Figure 5G). In summary, these data show that
365 enrichment of BCAM high-expressing CTB confers organoid growth and regenerative potential.

366

367

368 **DISCUSSION**

369 Here we applied single cell RNA sequencing of human placentas at two gestational age time-
370 points within the first trimester to further our understanding of human trophoblast development. In
371 doing this, we provide here novel transcriptomic data from 7,798 human trophoblasts, resolve the first
372 trimester trophoblast landscape at increased resolution, and clarify how gestational age informs
373 trophoblast heterogeneity, composition, and gene expression. To our knowledge, this is the first
374 trophoblast-focused study that accounts for multiple gestational age time-points within the first
375 trimester. Using state-of-the-art single cell lineage trajectory tools, we trace back the lineage
376 commitments made by developing CTBs to identify a novel trophoblast progenitor cell niche marked
377 by increased expression of the cell surface glycoprotein BCAM.

378 Previous studies have explored the maternal-placental interface transcriptome[18] as well as the
379 placental transcriptome across gestation at single cell resolution[22,23]. While these studies have
380 contributed important insight into placental cell heterogeneity, complexity, and have defined detailed
381 maternal-trophoblast interactions, a strict focus on understanding CTB hierarchy, the CTB progenitor
382 transcription factor regulatory landscape, and gene pathways underlying CTB commitment to EVT or
383 SCT has not been specifically addressed. Our study defines four CTB states. The first CTB state is
384 identified by increased expression of large (RPL) and small (RPS) ribosomal subunit genes.
385 Upregulation of these ribosomal subunit genes suggests increased ribosome content, and therefore
386 increased protein translation occurring within these cells[28]. Some studies have reported a link between
387 ribosomal subunit protein activity and regulation the cell cycle through P53-mediated arrest or the
388 promotion of proliferation[29]. The mixed expression of both activators (*RPS15A*[29]) and inhibitors
389 (*RPS14*[29]) of proliferation within this CTB state suggests that this cell state may represent a transient
390 CTB population increasing expression of ribosome genes to regulate entry into the cell cycle[28,29].
391 Further, previous work by Khajuria et al[30] has described a link between ribosome protein level and cell

392 differentiation, suggesting an alternative explanation that these cells are increasing expression of
393 ribosome subunits to facilitate differentiation out of the trophoblast stem cell state.

394 The second CTB state we define is a population of proliferative CTBs. Previous studies have
395 proposed that proliferating CTBs will generally contain trophoblast stem cells[23], allowing these
396 dividing cells to supply and replenish the placenta across gestation. Expression patterns of known
397 trophoblast stem cell markers, however, shows little overlap with these cells in our data, the exception
398 being *TEAD4*, which is identified as a potential key regulator of this state. Previous work has
399 demonstrated multiple roles for the TEA domain (TEAD) proteins in cell proliferation, differentiation,
400 and apoptosis[31-34]. Specifically, TEAD4 co-activation with VGLL1/2 proteins is shown to promote
401 proliferation, while TEAD4 co-activation with the Hippo pathway effector protein YAP has been
402 demonstrated to promote trophoblast stemness[24]. Comparison of the expression patterns of *TEAD4* and
403 *YAP1* (encoding the YAP protein), in our proliferative CTBs and in CTB2 suggests a dual role of
404 *TEAD4* expression in the CTB, dependent on the expression of these co-activators. Within our
405 proliferative CTBs, *TEAD4* is co-expressed with *VGLL1* without *YAP1*, demonstrating that here
406 TEAD4 is driving a proliferative and not stem phenotype.

407 The third CTB state identified is a metabolically active state, identified by increased expression
408 of mitochondria genes. Previous sequencing reports have noted that increased percent expression of
409 mitochondrial RNA may be indicative of cell stress or damage[35-37]. However, our quality control
410 pipeline filters on the basis of percent mitochondrial RNA content. As well, comparison of cell specific
411 feature detection and the detection of unique molecular identifiers indicates no observable difference
412 that would support the presence of damaged or dying cells. As a result, we theorize that these cells are
413 expressing mitochondrial RNA transcripts in response to increased metabolic demand. Unique to this
414 CTB state is the upregulation of many genes shown to be involved in trophoblast stemness, suggesting
415 a role for mitochondrial activity in CTB stemness. Fitting with this, recent work has shown a direct role

416 for WNT signaling in the promotion of CTB stemness[10-12], suggesting that these cells, which express a
417 CTB progenitor-like transcriptome but are not the CTB progenitors, may represent a transient CTB
418 state responding to WNT activation. To further support this hypothesis, recent work has demonstrated a
419 correlation between WNT activity and mitochondrial biogenesis/activation[38,39], however further work
420 is needed to test this in the placenta. Interestingly, three transcription factors were identified as master
421 regulators of this CTB state, ZBTB33, TFCP2L1, and FOXK1, all of which show involvement in the
422 regulation of WNT signaling.

423 We then sought to identify and characterize a trophoblast stem cell niche. Our initial approaches
424 involved branched pseudotime trajectory inference, which captured transitions between cell type as
425 CTB differentiate into SCT or EVT, however, this approach proved insufficient for delineating the
426 CTB specific developmental hierarchy. To circumvent this and identify the most primitive trophoblast
427 population, we applied a sophisticated RNA velocity approach for quantifying the relative amounts of
428 spliced and unspliced gene abundances. RNA velocity was able to identify CTB2, the fourth state, as
429 an origin population from which all trophoblasts arise. Within these cells, we observe increased
430 expression of the most primitive trophoblast stem cell gene *CDX2*, further indicating that these cells
431 represent a primitive CTB state. Gene ontology enrichment analysis of genes in CTB2 identified
432 biological process terms relating to hematopoietic progenitor cell differentiation and cellular response
433 to hypoxia. The first 9 weeks of gestation are characterized by a hypoxic oxygen concentration < 20
434 mm Hg that is maintained until maternal trophoblastic plugs are eroded at 10 weeks GA, bringing the
435 oxygen concentration of the maternal fetal interface to 40-80 mmHg[40-43]. Enrichment of hypoxia cell-
436 related terms within this origin indicates that these cells are highly sensitive to their environment, but
437 also that hypoxia-driven programs may play roles in coordinating progenitor functions in CTB. Indeed,
438 exposure to low levels of oxygen drive CTBs to differentiate into immature EVT[44-46], but the
439 contribution of hypoxia on progenitor biology is not as well developed. Future work aimed at

440 understanding the relationship between hypoxia and stemness in trophoblast development, including
441 the importance of HIF transcription factors in stem cell maintenance will be important.

442 Comparisons between our placental tissue sequencing data and our trophoblast organoid
443 sequencing data demonstrate similarities in general CTB, SCT and EVT function, but also subtle
444 differences between the different states of CTB found in each stem cell derived organoid condition and
445 our tissue CTBs. Comparison of the CTB progenitor niche identified in both the organoid and tissue
446 datasets identifies the common transcription factors *YAP1*, *SPINT2*, *PEG10*, and *MSI1* as well as
447 consistent upregulation of *BCAM*, supporting identification of BCAM as a CTB progenitor marker.
448 Interestingly, quantification of mRNA levels of known CTB related genes (*TEAD4* and *ITGA6*) as well
449 as SCT (*CGB* and *CSH1*) and EVT related genes (*ITGA5*, *NOTCH1*, *NOTCH2*, and *HLA-G*) on days 0,
450 11, and 21 of differentiation indicate that hTSC specific organoid colonies show different rates of
451 differentiation or capacities to differentiate. Our EVT-differentiated organoid transcriptomes were
452 sequenced on day 7 of differentiation, indicating that the differences we are observing may in part be
453 due to groups of organoid colonies being at a different stage of differentiation, with CT29 derived
454 organoids showing the most rapid capacity for EVT differentiation, followed by CT30 and CT27.

455 Consistent between our *in vivo* and *in vitro* datasets is the identification of two CTB progenitor
456 cell niches in the first trimester placenta, one representing a CTB origin state marked by increased
457 *BCAM* gene expression, and one representing a more specified bipotent EVT progenitor cell state,
458 marked by *ITGA2* and *NOTCH1* gene expression. Immunofluorescence microscopy and
459 immunohistochemistry of 8-9 week GA placental villi shows that ITGA2 is specific to proximal cells
460 within anchoring placental villi near the basement membrane[13]. It is thought that as chorionic villi
461 develop, trophoblast progenitors within close proximity to uterine stroma adopt a unique gene
462 expression profile that predisposes their differentiation trajectory to the extravillous pathway. We show
463 that the transcriptome of *ITGA2*$^{+}$ putative column progenitors express EVT-associated genes such as

464 *NOTCH1* and *ITGA5,* as well as the CTB/progenitor-associated genes *TFAP2C*, *GATA3*, and *ELF5*.
465 Lee et al[13] further describe ITGA2^{+} cCTBs as having a mixed endothelial- and mesenchymal-like
466 identity. This unique gene signature, harboring stem-like and EVT-like genes, supports the possibility
467 that *ITGA2*$^{+}$ CTB retain a level of bipotency. Analyses using scVelo trajectory inference suggests
468 *ITGA2*$^{+}$column/EVT progenitors descend from the *BCAM*$^{+}$ CTB progenitor origin and are maintained
469 as a reserve progenitor population within anchoring columns.

470 We identify *BCAM* as a gene expressed by CTB progenitors, where its expression is particularly
471 elevated in the most upstream CTB states. BCAM interacts predominantly with its ligand *LAMA5*, a
472 component of the laminin-511 heterotrimers found within the placental extracellular matrix[47,48]. BCAM
473 is an antigen upregulated in ovarian carcinoma, and facilitates tumor migration by competing for
474 laminin binding with integrins [49,50,51]. Here, we show that flow-cytometry enrichment of BCAM in
475 CTBs significantly potentiates CTB organoid growth. Interestingly, no differences were observed in the
476 capacity of BCAM^{hi} or BCAM^{lo} CTBs to form organoid colonies from single cells, suggesting that
477 BCAM^{hi} CTB may not have intrinsically greater stem-like properties over BCAM^{lo} CTB. Rather,
478 BCAM may enhance organoid growth by potentiating survival signals induced by cell-ECM
479 engagement, or by initiating/driving CTB proliferation pathways. However, we show that genes
480 associated with stem cell regeneration are elevated in BCAM^{hi} hTSC-derived organoids as compared to
481 organoids derived from BCAM^{lo} cells. Specifically, we show increased expression of *PEG10*, *EPCAM*,
482 and *HMGB3*, indicating that BCAM may confer increased organoid growth by controlling stem cell
483 maintenance or regeneration. In our experimental organoid system, even though BCAM^{lo} organoids
484 form smaller colonies by day 11, assessment of BCAM expression in BCAM^{lo} organoids at end-point
485 shows that BCAM levels and the frequency of BCAM-expressing cells is comparable to BCAM^{hi}
486 CTBs. This suggests that BCAM expression in progenitor CTBs is dynamic, and that requirements for
487 growth, stemness, or survival result in the induction of BCAM expression. Future work designed to

488 examine how BCAM drives trophoblast organoid growth will be necessary.

489

490 **SIGNIFICANCE**

491 The identification of a novel cell surface human CTB progenitor cell marker provides improved
492 methods for isolating and studying the mechanisms regulating human CTB progenitor cells, trophoblast
493 differentiation, and human placental development.

494

495 **CONCLUSIONS**

496 In conclusion, we have used single cell RNA sequencing to define trophoblast differentiation
497 trajectories in early human placental development. Importantly, we identify BCAM as a new CTB
498 progenitor marker that confers enhanced clonal growth. Future work is needed to clarify how increased
499 BCAM expression facilitates improved CTB growth, and the exact molecular paths through which this
500 occurs. We hope that future experiments will be able to capitalize on the identification of BCAM as a
501 cell surface CTB progenitor marker through which these cells can be isolated and further studied.

502

503 **MATERIALS AND METHODS**

504 **Patient recruitment and tissue collection**

505 Decidual and placental tissues were obtained with approval from the Research Ethics Board on
506 the use of human subjects, University of British Columbia (H13-00640). All samples were collected
507 from women (19 to 39 years of age) providing written informed consent undergoing elective
508 terminations of pregnancy at British Columbia's Women's Hospital, Vancouver, Canada. First
509 trimester placental tissues (*N*=7) were collected from participating women (gestational ages ranging
510 from 5–12 weeks) having confirmed viable pregnancies by ultrasound-measured fetal heartbeat. Patient
511 clinical characteristics i.e. height and weight were additionally obtained to calculate body mass index
512 (BMI: kg/m^2) and all consenting women provided self-reported information via questionnaire to having
513 first hand exposure to cigarette smoke or taken anti-inflammation or anti-hypertensive medications
514 during pregnancy. Patient and sample phenotype metadata are summarized in Supplemental Table 1.

515

516 **Human trophoblast organoids**

517 *Establishment and culture*: Human trophoblast stem cells (hTSC) CT27 (RCB4936), CT29
518 (RCB4937), and CT30 (RCB4938) from Riken BRC Cell Bank, were established from first–trimester
519 CTBs by Okae et al[10] and used here to generate organoid cultures using a modification of previously
520 described protocols[11,12]. In summary, these cells were re-suspended in ice-cold growth factor-reduced
521 Matrigel (GFR-M, Corning) to a final concentration of 100%. Cell suspensions (40µl) containing 5-20
522 x 10^3 cells were carefully seeded in the center of each well of a 24-well plate. Plates were placed at
523 37°C for 2 minutes. Following this, the plates were turned upside down to promote equal spreading of
524 the cells throughout the Matrigel domes. After 15 minutes, the plates were flipped back to normal and
525 the Matrigel domes were overlaid with 0.5mL pre-warmed trophoblast organoid media containing
526 advanced DMEM/F12 (Gibco), 10mM HEPES, 1 x B27 (Gibco), 1 x N2 (Gibco), 2mM L-glutamine

527 (Gibco), 100µg/ml Primocin (Invivogen), 100ng/mL R-spondin (PeproTech), 1µM A83-01 (Tocris),
528 100ng/mL rhEGF (PeproTech), 3µM CHIR99021 (Tocris), and 2µM Y-27632 (EMD Millipore).
529 Organoids were cultured for 7-21 days.

530 *EVT Differentiation*: EVT differentiation of trophoblast organoids was performed using an
531 adapted of previously published protocols[10]. In summary, organoids were cultured until > 50% colonies
532 reached at least 100µm in diameter (~3-5 days). Following this, organoids were maintained in EVT
533 differentiation media containing advanced DMEM/F12, 0.1mM 2-mercaptoethanol (Gibco), 0.5%
534 penicillin/streptomycin (Gibco), 0.3% BSA (Sigma Aldrich), 1% ITS-X supplement (Gibco),
535 100ng/mL NRG1 (Cell Signaling Technology), 7.5µM A83-01 (Tocris), 4% Knockout Serum
536 Replacement (Gibco). Media exchanged for EVT differentiation media lacking NRG1 around day 7-10
537 of differentiation following the visible outgrowth of cells. Differentiation was stopped at day 7 (D7) for
538 10X single cell RNA sequencing and flow cytometry analysis. Differentiation was stopped at day 21
539 (D21) for qPCR analysis.

540

541 **Placental tissue and trophoblast organoid single cell RNA-seq library construction**

542 *Placental tissue:* Healthy placental villi (BMI < 25.00 kg/m^2, MA: 20-32 years, and no
543 exposure to first hand cigarette smoke or anti-inflammation and anti-hypertensive medications during
544 pregnancy) were physically scraped form chorionic membrane by scalpel and enzymatically digested in
545 0.5ml collagenase/hyaluronidase and 1.5ml DMEM/F12 with 500µl penicillin/streptomycin and 500µl
546 100X antibiotic/antimycotic at 37˚C for 45 minutes. Placental villi cell suspensions were diluted in 1X
547 Hank's Balanced Salt Solution (HBSS) containing 2% FBS, pelleted at 1200rpm for 5 minutes, and
548 resuspended in 0.25% trypsin-EDTA. The solution was diluted again in 1X HBSS containing 2% FBS,
549 pelleted at 1200rpm for 5 minutes, and resuspended in dispase and 1mg/ml DNase I. 1X Hank's
550 Balanced Salt Solution (HBSS) containing 2% FBS was added once more and the solution was sieved

551 through a 40μm filter.

552 *Trophoblast organoids:* For all organoid cultures, media was aspirated and organoids were
553 diluted in Cell Recovery Solution at 4˚C for 40 minutes on either culture day 0 in complete media (for
554 non-differentiated organoids) or culture day 7 in differentiation media (for EVT-differentiated
555 organoids). Cells were then washed with cold PBS and centrifuged at 1000rpm for 5 minutes. Cells
556 were disaggregated in TrypLE containing 5% DNase I at 37˚C for 7 minutes before the addition of
557 100μl complete media. The resulting cell suspension was then sieved through a 40μm filter.

558 *Library construction*: Single cell suspensions (tissue- and organoid-derived) were stained with
559 7-Aminoactinomycin D (7-AAD) viability marker and live/dead sorted using a Becton Dickinson (BD)
560 FACS Aria. Cell suspensions were loaded onto the 10X Genomics single cell controller for library
561 preparation. Placental villi-derived single cell suspensions were prepared using the chromium single
562 cell 3' reagent v2 chemistry kit, following standard manufacturer protocol for all steps. Non-
563 differentiated and differentiated trophoblast organoid-derived single cell suspensions were prepared
564 using the chromium single cell 3' reagent v3 chemistry kit, following standard manufacturer protocol
565 for all steps. Single cell libraries were sequenced on an Illumina Nextseq 500 instrument at a
566 sequencing depth of 50,000 reads/cell for tissue-derived cells and 150,000 reads/cell for organoid-
567 derived cells. For placental villus samples, the 10X Genomics Cell Ranger version 2.0 software was
568 used for STAR read alignment and counting against the provided GRCh38 reference while the
569 trophoblast organoid samples used the 10X Genomics Cell Ranger version 3.0 software for STAR read
570 alignment and counting against the GRCh38 reference.

571 *Data Repository Integration*: Droplet-based first trimester scRNA-seq decidual and placental
572 tissue data was obtained from the public repository ArrayExpress (available at: E-MTAB-6701[18]). Raw
573 BAM files were downloaded and pre-processed using 10X Genomics Cell Ranger version 2.0 under
574 identical parameters as previously described for our placental villi and trophoblast organoid samples

575 using the GRCh38 reference. Sample specific metrics are summarized in Supplemental Table 2.

576

577 **Single cell RNA-seq data analysis**

578 *Data pre-processing and quality control*: A total of 50,790 single cells were sequenced and pre-
579 processed using the Seurat R package[52,53]. To ensure quality cells were used in downstream analyses,
580 cells containing fewer than 1000 detected genes and greater than 20% mitochondrial DNA content
581 were removed. Individual samples were scored based on expression of G2/M and S phase cell cycle
582 gene markers, scaled, normalized, and contaminating cell doublets were removed using the
583 DoubletFinder package[54] with default parameters and a doublet formation rate estimated from the
584 number of captured cells. Following pre-processing, all samples were merged and integrated using cell
585 pairwise correspondences between single cells across sequencing batches. During integration, the
586 Pearson residuals obtained from the default regularized negative binomial model were re-computed and
587 scaled to remove latent variation in percent mitochondrial DNA content as well as latent variation
588 resulting from the difference between the G2M and S phase cell cycle scores.

589 *Cell clustering, identification, and trophoblast sub-setting*: Cell clustering was accomplished in
590 Seurat at a resolution of 0.90 using 50 principal components. Cell identity was determined through
591 observation of known gene markers found within the maternal fetal interface (vimentin, CD45, neural
592 cell adhesion molecule, CD14, etc.) and identifying cluster marker genes via the "FindAllMarkers"
593 function using a model-based analysis of single-cell transcriptomics (MAST[55]) GLM-framework
594 implemented in Seurat. Gene markers were selected as genes with a minimum log fold change value >
595 0.20 and an adjusted p-value < 0.05 within a specific cluster. Trophoblasts were identified as
596 expressing *KRT7, EGFR, TEAD4, TP63, TFAP2A, TFAP2C, GATA2, GATA3, HLA-G, ERVFRD-1*
597 transcripts at a level greater than zero, and *VIM, WARS, PTPRC, DCN, CD34, CD14, CD86, CD163,*
598 *NKG7, KLRD1, HLA-DPA1, HLA-DPB1, HLA-DRA, HLA-DRB1, HLA-DRB5, HLA-DQA1* transcripts

599 at a level equal to zero. Trophoblasts were subset and re-clustered in Seurat at a resolution of 0.375
600 using 30 principal components. As mentioned previously, trophoblast cluster identity was determined
601 through observation of known trophoblast gene marker expression, proliferative gene marker
602 expression, and from unique cluster genes identified by differential expression analysis in Seurat.
603 Trophoblast projections were visualized using Uniform Manifold Approximation and Projections
604 (UMAPs).

605 *Differential gene expression*: Differential expression (DEG) analyses were performed in Seurat
606 using the "FindMarkers" function using a MAST framework on the raw count data. Parameters were
607 limited to genes with a log fold-change difference between groups of 0.20 and genes detected in a
608 minimum 10% cells in each group. Results were filtered for positive gene markers and significant
609 DEGs were taken as having a fold change difference > 0.25 and an adjusted p value < 0.05.

610 *Gene set enrichment analysis*: GSEA analyses were performed in Seurat using the
611 "FindMarkers" function using a MAST framework on the raw count data. Parameters included a
612 minimum log fold-change difference between groups of "−INF", a minimum gene detection of "−INF"
613 in cells in each group, and a minimum difference in the fraction of detected genes within each group of
614 "−INF", allowing all genes to be compared. Results were visualized using the R package
615 EnhancedVolcano (version 1.8.0), with a fold-change cut-off of 0.25 and a p value cut off of 0.00005
616 taken as the thresholds for significance.

617 *Gene ontology*: GO analysis of significant differentially expressed genes was performed using
618 the clusterProfiler R package[56] and the top enriched terms (Benjamini-Hochberg corrected p value
619 <0.05) were visualized as dot plots using the R package enrich plot (version 1.10.2).

620 *CTB gene regulatory network establishment*: Placental CTBs were subset and state-specific CTB gene
621 markers were identified as described in the *Differential gene expression* section, above. Results were
622 exported as an excel file for import into Cytoscape (version 3.7.1). State-specific, as well as aggregated

623 general CTB gene marker lists were imported as networks and the iRegulon package[59] was applied
624 using default parameters to define CTB gene regulatory networks.

625 *Pseudotime:* The Monocle2 R package[58-60] was used to explore the differentiation of progenitor
626 CTBs into specialized SCT and EVT. The trophoblast cell raw counts were loaded into Monocle2 for
627 semi-supervised single cell ordering in pseudotime, taking increased *BCAM* expression to represent
628 cells at the origin and *HLA-G* and *ERVFRD-1* gene expression to indicate progress towards EVT and
629 SCT, respectively. Branched expression analysis modelling (BEAM) was applied to observe the
630 expression of identified trophoblast cluster gene markers and genes related to the WNT, HIPPO,
631 NOTCH, and EGFR signaling pathways over pseudotime, progressing towards either EVT or SCT.
632 Results were visualized using the "plot_cell_trajectory" function. To resolve cytotrophoblast
633 differentiation trajectories at higher resolution, the Monocle3 package[61] was utilized. Trophoblast raw
634 counts were input, clustered, and the principal graph was created using the "learn_graph" function. The
635 "order_cells" function was then used to order cells in pseudotime, designating the trophoblast root
636 within the CTB 2 state.

637 *Lineage Trajectory*: The Velocyto package[62] was run in terminal using the command line
638 interface to generate sample-specific files containing count matrices of unspliced, spliced, and
639 ambiguous RNA transcript abundances. The velocyto.R implementation of the package was then used
640 to merge each file with its corresponding 10X sample during data pre-processing in Seurat. The final,
641 processed trophoblast object and UMAP embeddings were exported to a Jupyter Notebook and the
642 scVelo Python package[63] was used to read, prepare, and recover holistic trophoblast gene splicing
643 kinetics. Velocities were projected on top of the extracted UMAP embeddings generated in Seurat.

644 *Signaling Entropy*: The SCENT R package[64] was applied using default parameters and the
645 CCAT method for potency estimation to quantify the degree of differentiation potency and gene
646 expression promiscuity across single cells.

647

648 **Flow cytometry analysis and cell sorting**

649 *Organoid single cell work-flow*: Single cells from CT29 organoids were isolated by incubation
650 with Cell Recovery Solution (Corning) for 40 minutes at 4°C. Then, cells were washed in ice-cold PBS
651 and dissociated into single cells using TrypLE^{TM} supplemented with 5% DNAse I for 7 minutes at
652 37°C.

653 *Phenotyping EVT differentiated CT27, CT29, and CT30 organoids*: Following single cell
654 dissociation, organoid cells were stained with EGFR BV605 (clone AY13; 1:50; Biolegend), HLA-G
655 APC (clone MEMG-9; 1:50; Abcam), HLA-ABC Pacific Blue (clone W6/32; 1:100; Biolegend),
656 CD49e/ITGA5 PeCy7 (clone eBioGoH3; 1:200; Thermo Fisher Scientific), CD49f/ITGA6 Alexa 488
657 (clone P1D6; 1:200; Thermo Fisher Scientific), and BCAM BV711 (clone B64; 1:50; BD Biosciences).

658 *Phenotyping BCAM^{hi} and BCAM^{lo} organoids*: Single cells were incubated with anti-human
659 BCAM BV421 (clone B64; 1:50; BD Biosciences), EGFR BV605, and CD49f/ITGA6 PeCy7 for 30
660 minutes in the dark on ice, followed by viability staining with 7-AAD. Samples were analyzed using
661 LSRII (Becton Dickinson) and a minimum of 20,000 events were acquired.

662 *hTSC BCAM$^{hi/lo}$ sorting:* CT29 hTSCs were dissociated using TrypLE^{TM} (Thermo Fisher
663 Scientific) with 5% DNAse I (Sigma Aldrich) for 7 minutes at 37°C. Following resuspension in PBS
664 supplemented with Antibiotic-Antimycotic (Gibco) and 1% P/S (Sigma Aldrich), cells were stained
665 with BCAM BV421 (clone B64; 1:50; BD Biosciences) and EGFR Pecy7 (clone AY13; 1:50;
666 Biolegend) for 30 minutes at 4°C in the dark, followed by incubation with 7-AAD (Thermo Fisher) for
667 viability assessment. CT29 BCAM^{hi} and BCAM^{lo} populations were sorted using a FACS Aria (BD
668 Biosciences).

669

670

671 **Trophoblast organoid growth assay**

672 CT29 sorted BCAM^{hi} and BCAM^{lo} cells were seeded at a density of 5,000 cells in 40μL of
673 Matrigel in the presence of trophoblast organoid media. Phase contrast images were taken with
674 AxioObserver inverted microscope (Carl Zeiss) using 20X objective, and organoids were further
675 analyzed by qPCR, immunofluorescence, and flow cytometry. Organoid formation efficiency was
676 assessed by measuring organoid number and size (area in μm^2). Images were taken daily and analyzed
677 using imageJ (NIH). The scale was set by measuring the scale bar in pixels (285.5 pixels = 200μm).

678

679 **RNA isolation**

680 Prior to RNA extraction, organoids were dissociated into single cells as described above. Total
681 RNA was prepared from these cells using RiboZol reagent (VWR Life Science) followed by RNeasy
682 Mini kit (Qiagen) according to manufacturer's protocol. RNA purity was confirmed using a NanoDrop
683 Spectrophotometer (Thermo Fisher Scientific).

684

685 **cDNA synthesis and qPCR**

686 RNA was reverse transcribed using qScript cDNA SuperMix synthesis kit (Quanta Biosciences)
687 and subjected to qPCR (ΔΔCT) analysis, using PowerUP SYBR Green Master Mix (Thermo Fisher
688 Scientific) on a StepOnePlus Real-Time PCR System (Thermo Fisher Scientific) and forward and
689 reverse primer sets for *TEAD4* (F: 5'-CGGCACCATTACCTCCAACG-3'; R: 5'-
690 CTGCGTCATTGTCGATGGGC-3'), *ITGA6* (F: 5'-CACTCGGGAGGACAACGTGA-3'; R: 5'-
691 ACAGCCCTCCCGTTCTGTTG-3'), *CGB* (F: 5'-GCCTCATCCTTGGCGCTAGA-3'; R: 5'-
692 TATACCTCGGGGTTGTGGGG-3'), *CSH1* (F: 5'-GACTGGGCAGATCCTCAAGCA-3'; R: 5'-
693 CCATGCGCAGGAATGTCTCG-3'), *ITGA5* (F: 5'-GGGTCGGGGGCTTCAACTTA-3'; R: 5'-
694 ACACTGACCCCGTCTGTTCC-3'), *HLA-G* (F: 5'-CCCACGCACAGACTGACAGA-3'; R: 5'-

695 AGGTCGCAGCCAATCATCCA-3'), *NOTCH1* (F: 5'-GCCTGAATGGCGGGAAGTGT-3'; R: 5'-
696 TAGTCTGCCACGCCTCTGC-3'), *NOTCH2* (F: 5'-ACTCGGGGCCTACTCTGTGA-3'; R: 5'-
697 TGTCTCCCTCACAACGCTCC-3'), *GAPDH* (F: 5'-AGGGCTGCTTTTAACTCTGGT-3' R: 5'-
698 CCCCACTTGATTTTGGAGGGA-3'). All raw data were analyzed using StepOne Software v2.3
699 (Thermo Fisher Scientific). The threshold cycle values were used to calculate relative gene expression
700 levels. Values were normalized to endogenous *GAPDH* transcripts.
701
702 **Immunofluorescence microscopy**
703 Placental villi (6-12 weeks' gestation; n=2) were fixed in 2% paraformaldehyde overnight at 4
704 °C. Tissues were paraffin embedded and sectioned at 6 μm onto glass slides. Immunofluorescence was
705 performed as previously described (Aghababaei et al., 2015). Briefly, organoids or placental tissues
706 underwent antigen retrieval by heating slides in a microwave for 5 X 2 minute intervals in citrate buffer
707 (pH 6.0). Sections were incubated with sodium borohydride for 5 minutes at room temperature (RT),
708 followed by Triton X-100 permeabilization for 5 minutes, RT. Slides were blocked in 5% normal goat
709 serum/0.1% saponin for 1hr, RT, and incubated with combinations of the indicated antibodies
710 overnight at 4 °C: mouse monoclonal anti-HLA-G (clone 4H84; 1:100; Exbio, Vestec, Czech
711 Republic); rabbit monoclonal anti-cytokeratin 7 (clone SP52; 1:50; Ventana Medical Systems), rabbit
712 polyclonal anti-BCAM (1:100; Abcam); mouse monoclonal anti-hCG beta (clone 5H4-E2; 1:100;
713 Abcam). Following overnight incubation, sections and coverslips were washed with PBS and incubated
714 with Alexa Fluor goat anti-rabbit 568 and goat anti-mouse 488 conjugated secondary antibodies (Life
715 Technologies, Carlsbad, CA) for 1h at RT, washed in PBS and mounted using ProLong Gold mounting
716 media containing DAPI (Life Technologies).
717 Slides were imaged with an AxioObserver inverted microscope (Car Zeiss, Jena, Germany)
718 using 20X Plan-Apochromat/0.80NA or 40X Plan-Apochromat oil/1.4NA objectives (Carl Zeiss). An

719 ApoTome .2 structured illumination device (Carl Zeiss) set at full Z-stack mode and 5 phase images
720 was used for image acquisition.
721
722 **Statistical analysis**
723 Data are reported as median values with standard deviations. All calculations were carried out
724 using GraphPad Prism software (San Diego, CA). For single comparisons, Mann-Whitney non-
725 parametric unpaired t-tests were performed. For multiple comparisons, one-way Kruskal-Wallis
726 ANOVA followed by Dunn's multiple comparison test was performed. One-way ANOVA followed by
727 Tukey post-test were performed for all other multiple comparisons. The differences were accepted as
728 significant at $P < 0.05$. For scRNA-seq statistical analyses, please refer to scRNA-seq analysis sections
729 in methods.
730
731

732 **DATA AVAILABILITY/ACCESSION NUMBER**

733 The ArrayExpress accession number for the publicly available data reported in this paper is: E-
734 MTAB-6701.

735

736 **AUTHOR CONTRIBUTIONS**

737 AGB designed the research. AGB, MS, JB, BC, JW, SY, JT, and HTL performed experiments
738 and analysed data. AGB, MS, JB, and BC wrote the paper. All authors read and approved the
739 manuscript.

740

741 **FUNDING**

742 This work was supported by a Natural Sciences and Engineering Research Council of Canada
743 (NSERC; RGPIN-2014-04466) Discovery Grant (to AGB), Canadian Institutes of Health Research
744 201809PJT-407571-CIA-CAAA) operating grants to AGB, and a CIHR Master's graduate studentship
745 (to MS).

746

747 **ACKNOWLEDGEMENTS**

748 The authors extend their sincere gratitude to the hard work of staff at British Columbia's
749 Women's Hospital's CARE Program for recruiting participants to our study and the staff at the
750 University of British Columbia Biomedical Research Centre for assistance with all drop-seq library
751 preparation and sequencing.

752

753 **COMPETING INTERESTS**

754 The authors declare that no competing interests exist.

755

REFERENCES

1. Lee CQE, et al. What is a trophoblast? A combination of criteria define human first-trimester trophoblast. *Stem Cell Reports*. 2016. 6(2): 257-272. Doi: 10.1016/j.stemcr.2016.01.006.
2. Chang CW, et al. Trophoblast lineage specification, differentiation, and their regulation by oxygen tension. *J Endocrinol*. 2018. 236(1): R43-56. Doi: https://doi.org/10.1530/JOE-17-0402.
3. Pjinenborg R, et al. Deep placentation. *Best Pract Res Clin Obstet Gynaecol*. 2011. 25(3): 273-285. Doi: 10.1016/j.bpobgyn.2010.10.009.
4. Burton GJ, et al. Review Histotrophic nutrition and the placental-endometrial dialogue during human early pregnancy. *Placenta*. 2020 102: 21-26. Doi: 10.1016/j.placenta.2020.02.008.
5. Tilburgs T, et al. Human HLA-G+ extravillous trophoblasts: Immune-activating cells that interact with decidual leukocytes. *Proc Natl Acad Sci USA*. 2015. 112(23): 7219-7224. Doi: 10.1073/pnas.1507977112.
6. Turco MY and Moffett A. Development of the human placenta. *Development*. 2019. 146(22): dev163428. Doi: 10.1242/dev.163428.
7. Fowden AL, et al. Review: Endocrine regulation of placental phenotype. *Placenta*. 2015. 36 Suppl 1: S50-59. Doi: 10.1016/j.placenta.2014.11.018.
8. Geusens N, et al. Endovascular trophoblast invasion, spiral artery remodelling and uteroplacental haemodynamics in a transgenic rat model of pre-eclampsia. *Placenta*. 2008. 29(7): 614-623. Doi: 10.1016/j.placenta.2008.04.005.
9. Knöfler M, et al. Human placenta and trophoblast development: key molecular mechanisms and model systems. *Cell Mol Life Sci*. 2019. 76(18): 3479-3496. Doi: 10.1007/s00018-019-03104-6.
10. Okae, et al. Derivation of Human Trophoblast Stem Cells. *Cell Stem Cell*. 2018. 22(1): 50-63.e6. Doi: 10.1016/j.stem.2017.11.004.
11. Haider S, et al. Self-Renewing Trophoblast Organoids Recapitulate the Developmental Program of the Early Human Placenta. *Stem Cell Reports*. 2018. 11(2): 537-551. Doi: 10.1016/j.stemcr.2018.07.004.
12. Turco MY, et al. Trophoblast organoids as a model for maternal-fetal interactions during human placentation. *Nature*. 2018. 564(7735): 263-267. Doi: 10.1038/s41586-018-0753-3.
13. Lee CQE, et al. Integrin α2 marks a niche of trophoblast progenitor cells in first trimester human placenta. *Development*. 2018. 145(16): dev162305. Doi: 10.1242/dev.162305.
14. Pollheimer J, et al. Regulation of Placental Extravillous Trophoblasts by the Maternal Uterine Environment. *Front Immunol*. 2018. 9: 2597. Doi: 10.3389/fimmu.2018.02597.

788 **15.** Papuchova H, et al. Three types of HLA-G+ extravillous trophoblasts that have distinct immune
789 regulatory properties. *Proc Natl Acad Sci USA*. 2020. 117(27): 15772-15777. Doi:
790 10.1073/pnas.2000484117.
791 **16.** Moffett A, et al. Maternal allo-recognition of the fetus. *Fertil Steril*. 2017 107(6): 1269-1272. Doi:
792 10.1016/j.fertnstert.2017.05.001.
793 **17.** Jauniaux E, et al. Placental Implantation Disorders. *Obstet Gynecol Clin North Am*. 2020. 47(1):
794 117-132. Doi: 10.1016/j.ogc.2019.10.002.
795 **18.** Vento-Tormo R, et al. Single-cell reconstruction of the early maternal-fetal interface in humans.
796 *Nature*. 2018. 563 (7731): 347-353. Doi: 10.1038/s41586-018-0698-6.
797 **19.** Haider S, et al. Notch1 controls development of the extravillous trophoblast lineage in the human
798 placenta. *Proc Natl Acad Sci USA*. 2016. 113(48): E7710-E7719. Doi: 10.1073/pnas.1612335113.
799 **20.** Zhou Y, et al. Human cytotrophoblasts adopt a vascular phenotype as they differentiate. A strategy
800 for successful endovascular invasion? *J Clin Invest*. 1997. 99(9): 2139-2151. Doi:
801 10.1172/JCI119387.
802 **21.** Haider S, et al. Notch signaling plays a critical role in motility and differentiation of human first-
803 trimester cytotrophoblasts. *Endocrinology*. 2014. 155(1): 263-74. Doi: 10.1210/en.2013-1455.
804 **22.** Suryawanshi H, et al. A single-cell survey of the human first-trimester placenta and decidua. *Sci*
805 *Adv*. 2018. 4(10):eaau4788. Doi: 10.1126/sciadv.aau4788.
806 **23.** Liu Y, et al. Single-cell RNA-seq reveals the diversity of trophoblast subtypes and patterns of
807 differentiation in the human placenta. *Cell Res*. 2018. 28(8):8 19-832. Doi: 10.1038/s41422-018-
808 0066-y.
809 **24.** Meinhardt G, et al. Pivotal role of the transcriptional co-activator YAP in trophoblast stemness of
810 the developing human placenta. *Proc Natl Acad Sci USA*. 2020. 117(24): 13562-13570. Doi:
811 10.1073/pnas.2002630117.
812 **25.** Saha B, et al. TEAD4 ensures postimplantation development by promoting trophoblast self-
813 renewal: An implication in early human pregnancy loss. *Proc Natl Acad Sci USA*. 2020. 117(30):
814 17864-17875. Doi: 10.1073/pnas.2002449117.
815 **26.** Del Valle-Pérez B, et al. Wnt controls the transcriptional activity of Kaiso through CK1ε-dependent
816 phosphorylation of p120-catenin. *J Cell Sci*. 2016. 129(4): 873. Doi: 10.1242/jcs.186288.
817 **27.** Nemeth MJ, et al. Hmgb3 regulates the balance between hematopoietic stem cell self-renewal and
818 differentiation. *Proc Natl Acad Sci USA*. 2006. 103(37): 13783-8. Doi: 10.1073/pnas.0604006103.
819 **28.** Thomas G. An encore for ribosome biogenesis in the control of cell proliferation. *Nature*. 2000. 2:

820 E71-72.
821 **29.** Xu X, et al. The role of ribosomal proteins in the regulation of cell proliferation, tumorigenesis, and
822 genomic integrity. *Sci China Life*. 2016. 59(7): 656-672.
823 **30.** Khajuria RK, et al. Ribosome levels selectively regulate translation and lineage commitment in
824 human hematopoiesis. *Cell*. 2018. 173(1): Doi: 10.1016/j.cell.2018.02.036.
825 **31.** Shi Z, et al. DNA-binding mechanism of the Hippo pathway transcription factor TEAD4.
826 *Oncogene*. 2017. 36: 4362-4369. Doi: https://doi.org/10.1038/onc.2017.24.
827 **32.** Saha B, et al. TEAD4 ensures postimplantation development by promoting trophoblast self-
828 renewal: an implication in early human pregnancy loss. PNAS. 2020. 117(30): 17864-17875.
829 **33.** Xiao L, et al. Deciphering a distinct regulatory network of TEAD4, CDX2 and GATA3 in humans
830 for trophoblast transition from embryonic stem cells. *Biochim Biophys Acta Mol Cell Res*. 2020.
831 1867(9): 118736.
832 **34.** Yagi R, et al. Transcription factor TEAD4 specifies the trophectoderm lineage at the beginning of
833 mammalian development. *Development*. 2007. 134: 3827-3836. doi: 10.1242/dev.010223.
834 **35.** Ilicic T, et al. Classification of low quality cells from single-cell RNA-seq data. *Genome Biol*.
835 2016. 17(29). Doi: https://doi.org/10.1186/s13059-016-0888-1.
836 **36.** Galluzzi L, et al. Mitochondria: master regulators of danger signalling. *Nat Rev Mol Cell Biol*.
837 2012. 13: 780-788. Doi: https://doi.org/10.1038/nrm3479.
838 **37.** Detmer SA and Chan DC. Functions and dysfunctions of mitochondrial dynamics. *Nat Rev Mol*
839 *Cell Biol*. 2007. 8: 870-879. Doi: https://doi.org/10.1038/nrm2275.
840 **38.** Yoon JC, et al. Wnt signaling regulates mitochondrial physiology and insulin sensitivity. *Genes &*
841 *Dev*. 2010. 24: 1507-1518. Doi: 10.1101/gad.1924910.
842 **39.** Brown K, et al. WNT/β-catenin signaling regulates mitochondrial activity to alter the oncogenic
843 potential of melanoma in a PTEN-dependent manner. *Oncogene*. 2017. 36(22): 3119-3136. Doi:
844 10.1038/onc.2016.450.
845 **40.** Jauniaux E, et al. Onset of maternal arterial blood flow and placental oxidative stress. A possible
846 factor in human early pregnancy failure. *Am J Pathol*. 2000. 157(6): 2111-2122. Doi:
847 10.1016/S0002-9440(10)64849-3.
848 **41.** Jauniaux E, et al. Evaluation of respiratory gases and acid-base gradients in human fetal fluids and
849 uteroplacental tissue between 7 and 16 weeks' gestation. *Am J ObGyn*. 2001. 184(5): 998-1003.
850 **42.** Weiss G, et al. The trophoblast plug during early pregnancy: a deeper insight. *Histochem Cell Biol*.
851 2016. 146: 749-756. Doi: https://doi.org/10.1007/s00418-016-1474-z.

852 **43.** Tuuli MG, et al. Review: oxygen and trophoblast biology—a source of controversy. Placenta. 2011.
853 32(2): S109-S118. doi: 10.1016/j.placenta.2010.12.013.
854 **44.** Chang CW, et al. Trophoblast lineage specification, differentiation, and their regulation by oxygen
855 tension. J Endocrinol. 2018. 236(1): R43-56. Doi: https://doi.org/10.1530/JOE-17-0402.
856 **45.** Wakeland AK, et al. Hypoxia directs human extravillous trophoblast differentiation in a hypoxia-
857 inducible factor-dependent manner. Am J Pathol. 2017. 187(4): 767-780. Doi:
858 https://doi.org/10.1016/j.ajpath.2016.11.018.
859 **46.** Treissman J, et al. Low oxygen enhances trophoblast column growth by potentiating differentiation
860 of the extravillous lineage and promoting LOX activity. Development. 2020. 147(2). DOI:
861 10.1242/dev.181263.
862 **47.** Zen Q, et al. Critical factors in basal cell adhesion molecule/Lutheran-mediated adhesion to
863 laminin. J Biol Chem. 1999. 274(2): 728-734. Doi: https://doi.org/10.1074/jbc.274.2.728.
864 **48.** Kikkawa Y, et al. The Lutheran/basal cell adhesion molecule promotes tumor cell migration by
865 modulating integrin-mediated cell attachment to laminin-511 protein. J Biol Chem. 288(43): 30990-
866 31001. Doi: https://doi.org/10.1074/jbc.M113.486456.
867 **49.** Kannan K et al. Recurrent BCAM-AKT2 fusion gene leads to a constitutively activated AKT2
868 fusion kinase in high-grade serous ovarian carcinoma. PNAS. 2015. 112(11): E1272-1277. Doi:
869 10.1073/pnas.1501735112.
870 **50.** Jin J, et al. Upregulation of BCAM and its sense lncRNA BAN are associated with gastric cancer
871 metastasis and poor prognosis. Mol Oncology. 2020. 14(4): 829-845. Doi:
872 https://doi.org/10.1002/1878-0261.12638.
873 **51.** Akiyama H, et al. The FBI/Akirin2 target gene, BCAM, acts as a suppressive oncogene. PLOS
874 One. 2013. 8(11): e78716. Doi: https://doi.org/10.1371/journal.pone.0078716.
875 **52.** Butler A, et al. Integrating single-cell transcriptomic data across different conditions, technologies,
876 and species. *Nature Biotechnol*. 2018. 36(5): 411-420.
877 **53.** Stuart T, et al. Comprehensive integration of single-cell data. *Cell*. 2019. 177(7): 1888-1902.
878 **54.** McGinnis CS, et al. DoubletFinder: Doublet detection in single-cell RNA sequencing data using
879 artificial nearest neighbours. Cell Systems. 2019. 8(4): 329-337.
880 **55.** Finak G, et al. MAST: a flexible statistical framework for assessing transcriptional changes and
881 characterizing heterogeneity in single-cell RNA sequencing data. *Genome Biol*. 2015. 16: 278.
882 **56.** Yu G, et al. clusterProfiler: an R package for comparing biological themes among gene clusters.
883 *OMICS*. 2012. 16(5): 284-287.

884 **57.** Janky R, et al. iRegulon: from a gene list to a gene regulatory network using large motif and track
885 collections. *PLoS Comput Biol*. 2014. 10(7): e1003731.
886 **58.** Trapnell C, Cacchiarella D, et al. The dynamics and regulators of cell fate decisions are revealed by
887 pseudo-temporal ordering of single cells. *Nature Biotechnol*. 2014. 32(4): 381.
888 **59.** Qiu X, Hill A, Trapnell C, et al. Single-cell mRNA quantification and differential analysis with
889 Census. *Nat Methods*. 2017. 14(3): 309-315.
890 **60.** Qiu X, Trapnell C, et al. Reverse graph embedding resolves complex single-cell developmental
891 trajectories. *Nat Methods*. 2017. 14(10): 979-982.
892 **61.** Cao J, et al. The single-cell transcriptional landscape of mammalian organogenesis. *Nature*. 2019.
893 566(7745): 496-502. Doi: 10.1038/s41586-019-0969-x.
894 **62.** La Manno G, et al. RNA velocity of single cells. *Nature*. 2018. 560: 494-498.
895 **63.** Bergen V, et al. Generalizing RNA velocity to transient cell states through dynamical modelling.
896 Nature Biotechnol. 2020: https://doi.org/10.1038/s41587-020-0591-3
897 **64.** Teschendorff A, Enver T. Single-cell entropy for accurate estimation of differentiation potency
898 from a cell's transcriptome. *Nat Commun*. 2017. 8(1): 1-15.

899

900 **TITLES AND LEGENDS TO FIGURES**

901 **Figure 1: Single cell characterization of first trimester trophoblasts**
902
903 **(A)** Schematic of a first trimester chorionic villous including anatomical representations of both an
904 anchoring villous and floating villous. Highlighted are trophoblast sub-populations and the villous and
905 extravillous cell differentiation trajectories: cytotrophoblast (CTB), column cytotrophoblast (cCTB),
906 syncytiotrophoblast (SCT), and invasive extravillous trophoblast (EVT).
907 **(B)** Summary of workflow used for collection, processing, and single cell analysis of placental villous
908 cells. MFI, Maternal-Fetal Interface, 7AAD: 7-Aminoactinomycin D, FSC-A: Forward Scatter Area.
909 **(C)** Uniform Manifold Approximation and Projection (UMAP) plot of 7798 captured trophoblasts,
910 demonstrating 8 distinct trophoblast clusters: CTB1-4, cCTB1-2, SCTp, and EVT.
911 **(D)** Heatmap showing the average expression of known trophoblast and proliferation gene markers in
912 each trophoblast cluster. Cell cluster names and colours correspond to those in Figure 1C.
913 **(E)** Stacked bar plot showing cell state distribution in distinct phases of the cell cycle (G1, G2M, S).
914 **(F)** UMAP plots showing expression (red) of CTB progenitor (*EGFR*, *TP63*), proliferation (*MKI67*),
915 EVT (*HLA-G*), SCT (*ERVFRD-1*), and an EVT progenitor (*ITGA2*) gene(s).
916 **(G)** Proportion of 4687 early first trimester trophoblasts in each scRNA-seq-defined state in early (6-7
917 weeks) and late (9-12 weeks) gestational time-points.

Figure 1

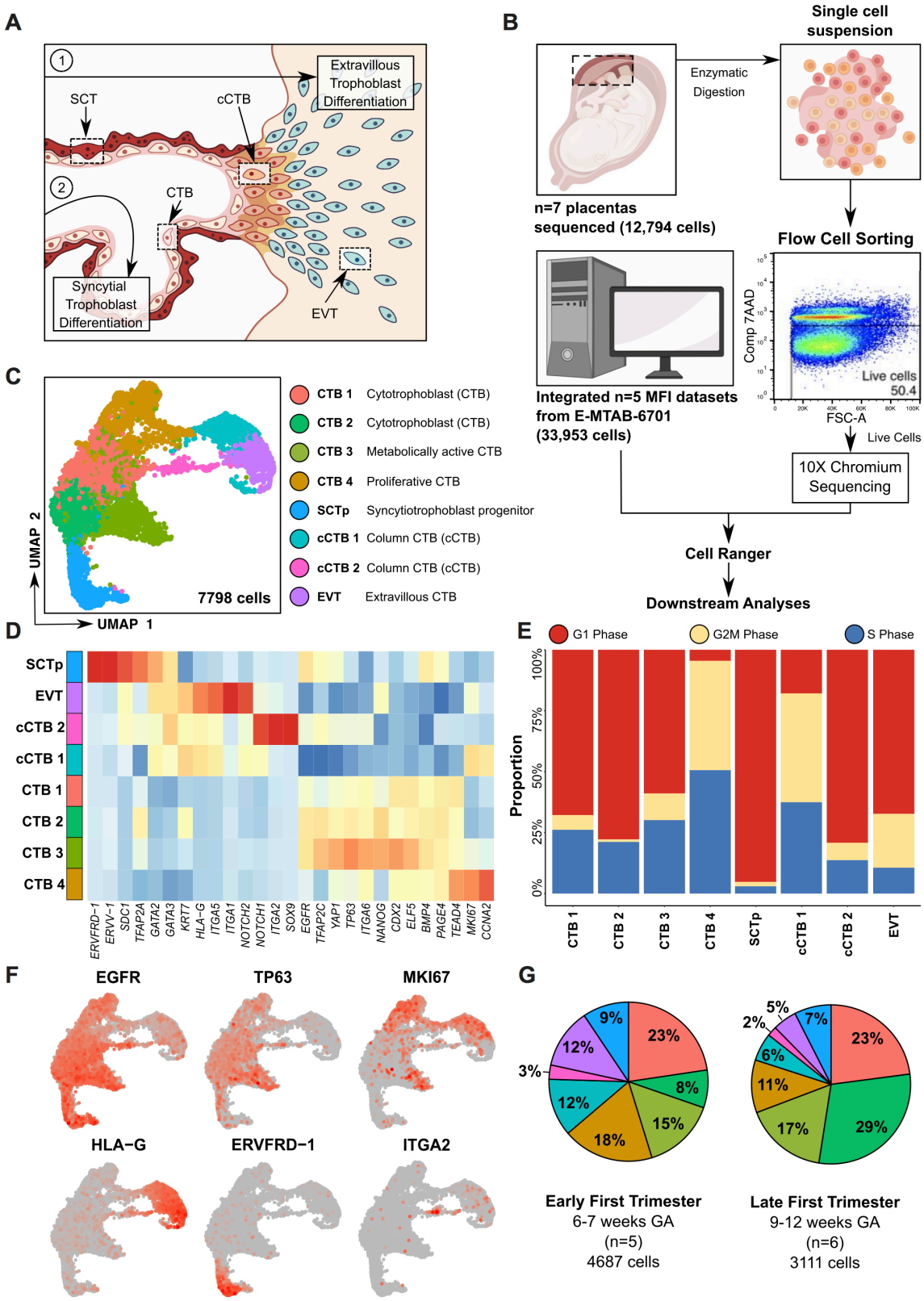
A
1
Extravillous Trophoblast Differentiation
SCT
cCTB
2
CTB
Syncytial Trophoblast Differentiation
EVT
B
Single cell suspension
Enzymatic Digestion
n=7 placentas sequenced (12,794 cells)
Flow Cell Sorting
Comp 7AAD
Live cells 50.4
FSC-A
Live Cells
Integrated n=5 MFI datasets from E-MTAB-6701 (33,953 cells)
10X Chromium Sequencing
Cell Ranger
Downstream Analyses
C
UMAP 2
UMAP 1
7798 cells
CTB 1 Cytotrophoblast (CTB)
CTB 2 Cytotrophoblast (CTB)
CTB 3 Metabolically active CTB
CTB 4 Proliferative CTB
SCTp Syncytiotrophoblast progenitor
cCTB 1 Column CTB (cCTB)
cCTB 2 Column CTB (cCTB)
EVT Extravillous CTB
D
SCTp
EVT
cCTB 2
cCTB 1
CTB 1
CTB 2
CTB 3
CTB 4
ERVFRD−1 ERVV−1 SDC1 TFAP2A GATA2 GATA3 KRT7 HLA−G ITGA5 ITGA1 NOTCH2 NOTCH1 ITGA2 SOX9 EGFR TFAP2C YAP1 TP63 ITGA6 NANOG CDX2 ELF5 BMP4 PAGE4 TEAD4 MKI67 CCNA2
E
G1 Phase
G2M Phase
S Phase
Proportion
0% 25% 50% 75% 100%
CTB 1 CTB 2 CTB 3 CTB 4 SCTp cCTB 1 cCTB 2 EVT
F
EGFR
TP63
MKI67
HLA−G
ERVFRD−1
ITGA2
G
23% 8% 15% 18% 12% 3% 12% 9%
Early First Trimester
6-7 weeks GA
(n=5)
4687 cells
23% 29% 17% 11% 6% 2% 5% 7%
Late First Trimester
9-12 weeks GA
(n=6)
3111 cells

Figure 2: Single cell transcriptomic resolution of distinct CTB states

(A) UMAP plot of 5477 captured CTBs highlighting 4 distinct cell states (CTB1-4).
(B) Heatmap showing the average expression of the top-10 most highly-expressed (FDR-ranked) genes in CTB states 1-4.
(C) Venn diagram comparing the intersection of genes upregulated within each CTB1-4 states.
(D) Dot plots of the top significant terms enriched by gene ontology analysis informed by gene signatures enriched within distinct CTB (CTB1-4) states.
(E) Heatmap showing the average expression of transcription factors identified as putative regulators/drivers enriched within CTB1-4 states.

Figure 2

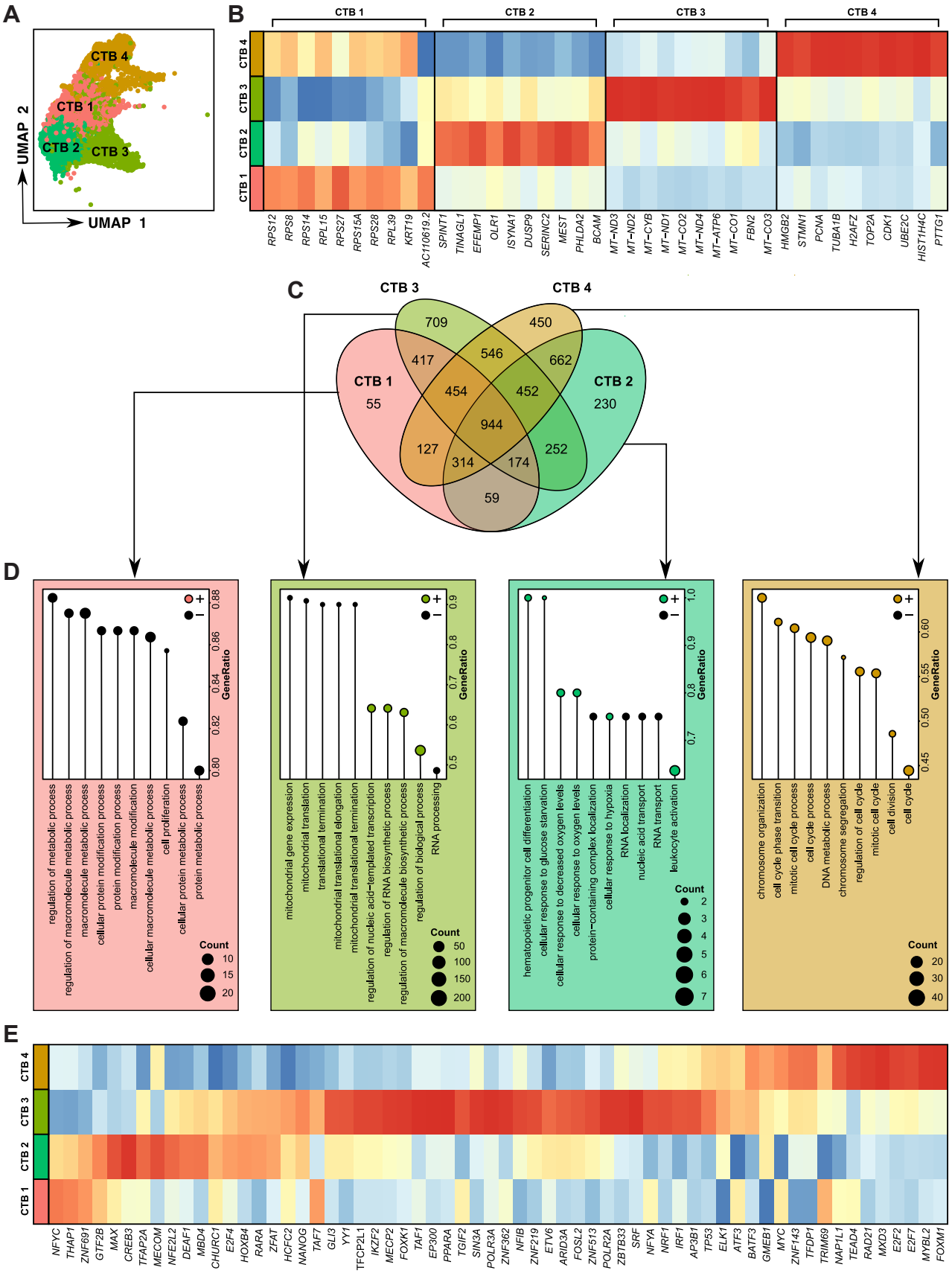
A
CTB 4
CTB 1
CTB 2
CTB 3
UMAP 2
UMAP 1
B
CTB 1
CTB 2
CTB 3
CTB 4
RPS12 RPS8 RPS14 RPL15 RPS27 RPS15A RPS28 RPL39 KRT19 AC110619.2
SPINT1 TINAGL1 EFEMP1 OLR1 ISYNA1 DUSP9 SERINC2 MEST PHLDA2 BCAM
MT-ND3 MT-ND2 MT-CYB MT-ND1 MT-CO2 MT-ND4 MT-ATP6 MT-CO1 FBN2 MT-CO3
HMGB2 STMN1 PCNA TUBA1B H2AFZ TOP2A CDK1 UBE2C HIST1H4C PTTG1
C
CTB 3
CTB 4
CTB 1
55
CTB 2
230
709
450
417
546
662
454
452
944
127
252
314
174
59
D
regulation of metabolic process
regulation of macromolecule metabolic process
macromolecule metabolic process
cellular protein modification process
protein modification process
macromolecule modification
cellular macromolecule metabolic process
cell proliferation
cellular protein metabolic process
protein metabolic process
GeneRatio
Count
mitochondrial gene expression
mitochondrial translation
translational termination
mitochondrial translational elongation
mitochondrial translational termination
regulation of nucleic acid-templated transcription
regulation of RNA biosynthetic process
regulation of macromolecule biosynthetic process
regulation of biological process
RNA processing
hematopoietic progenitor cell differentiation
cellular response to glucose starvation
cellular response to decreased oxygen levels
cellular response to oxygen levels
protein-containing complex localization
cellular response to hypoxia
RNA localization
nucleic acid transport
RNA transport
leukocyte activation
chromosome organization
cell cycle phase transition
mitotic cell cycle process
cell cycle process
DNA metabolic process
chromosome segregation
regulation of cell cycle
mitotic cell cycle
cell division
cell cycle
E
CTB 1
CTB 2
CTB 3
CTB 4
NFYC THAP1 ZNF691 GTF2B MAX CREB3 TFAP2A MECOM NFE2L2 DEAF1 MBD4 CHURC1 E2F4 HOXB4 RARA ZFAT HCFC2 NANOG TAF7 GLI3 YY1 TFCP2L1 IKZF2 MECP2 FOXK1 TAF1 EP300 PPARA TGIF2 SIN3A POLR3A ZNF362 NFIB ZNF219 ETV6 ARID3A FOSL2 ZNF513 POLR2A ZBTB33 SRF NFYA NRF1 IRF1 AP3B1 TP53 ELK1 ATF3 BATF3 GMEB1 MYC ZNF143 TFDP1 TRIM69 NAP1L1 TEAD4 RAD21 MXD3 E2F2 E2F7 MYBL2 FOXM1

929 **Figure 3: scVelo-informed cell differentiation identifies a primitive CTB origin.**
930
931 **(A)** UMAP plot overlain with projected RNA velocity (scVelo) vector field, indicating trophoblast
932 directionality (represented by the velocity arrows) away from a putative origin towards endpoint SCTp
933 and EVT states. Cell cluster names and colours correspond to those in Figure 1C.
934 **(B)** UMAP plots showing gene expression (red) of progenitor- and stem cell-associated genes in all
935 scRNA-seq-informed trophoblast states.
936 **(C)** Venn diagram comparing the genes upregulated within CTB states 2 and 3. Highlighted are genes
937 related to WNT and EGFR signaling pathways, genes involved in extracellular matrix (ECM)
938 interactions, and miscellaneous (Misc) genes of interest.
939 **(D)** Scatter plots showing gene expression levels of EGFR related genes (*EFEMP1*), transcription
940 factors (*EGR1* and *ELF5*), and genes involved in ECM-cell interactions (*ITGA6*, *BCAM*, and *LAMA5*)
941 across pseudotime as the CTB2 state transitions to the CTB3 state.
942 **(E)** UMAP plots showing gene expression (red) of genes upregulated within the CTB2 state origin.
943

Figure 3

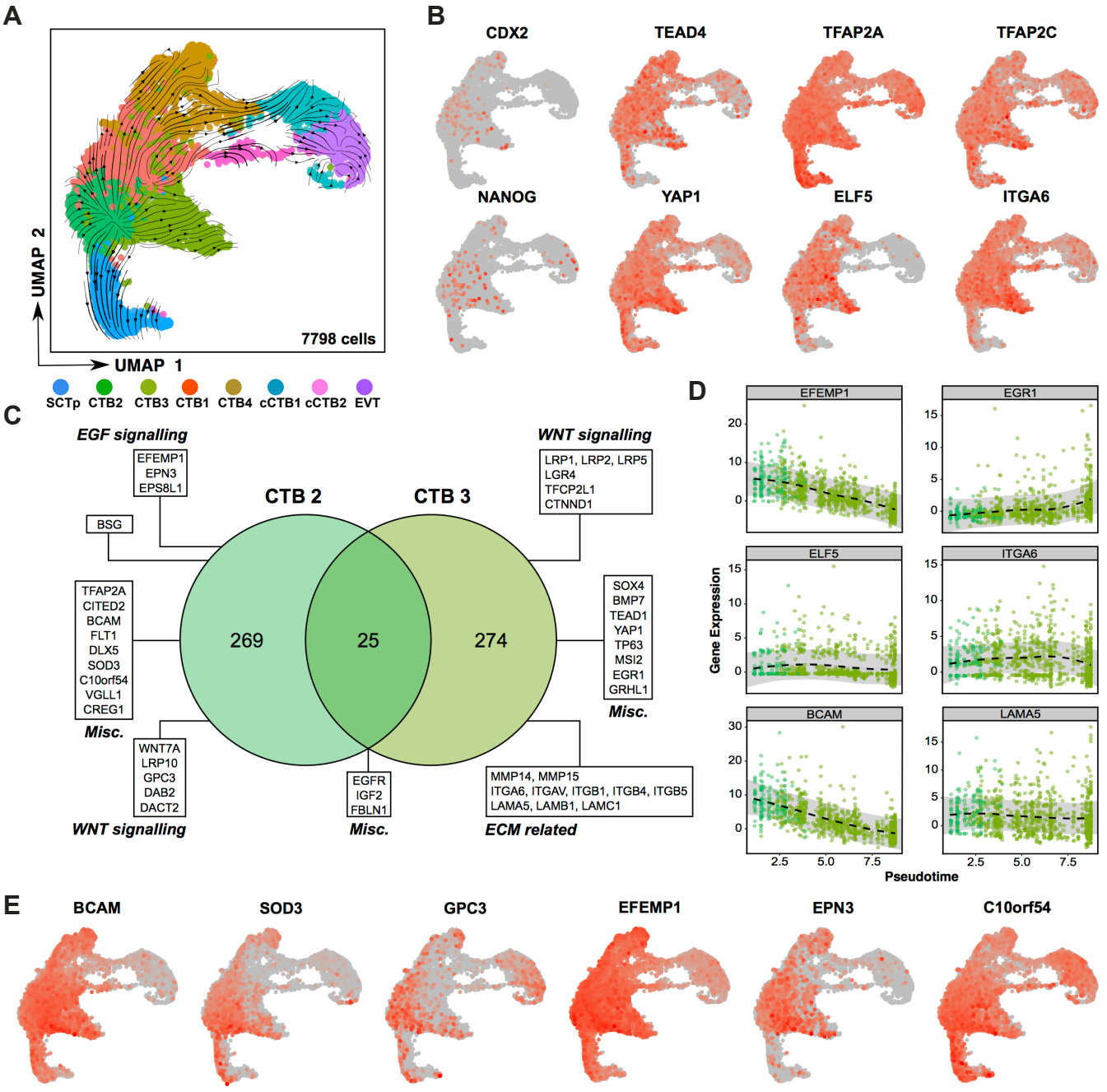
A
UMAP 2
UMAP 1
7798 cells
SCTp CTB2 CTB3 CTB1 CTB4 cCTB1 cCTB2 EVT
B
CDX2
TEAD4
TFAP2A
TFAP2C
NANOG
YAP1
ELF5
ITGA6
C
EGF signalling
EFEMP1
EPN3
EPS8L1
BSG
WNT signalling
LRP1, LRP2, LRP5
LGR4
TFCP2L1
CTNND1
CTB 2
CTB 3
269
25
274
TFAP2A
CITED2
BCAM
FLT1
DLX5
SOD3
C10orf54
VGLL1
CREG1
Misc.
SOX4
BMP7
TEAD1
YAP1
TP63
MSI2
EGR1
GRHL1
Misc.
WNT7A
LRP10
GPC3
DAB2
DACT2
WNT signalling
EGFR
IGF2
FBLN1
Misc.
MMP14, MMP15
ITGA6, ITGAV, ITGB1, ITGB4, ITGB5
LAMA5, LAMB1, LAMC1
ECM related
D
EFEMP1
EGR1
ELF5
ITGA6
BCAM
LAMA5
Gene Expression
Pseudotime
E
BCAM
SOD3
GPC3
EFEMP1
EPN3
C10orf54

Figure 4: Single cell transcriptomic analyses in hTSC organoids recapitulate a primitive CTB origin

(A) Bright field microscopy images of regenerative (Wnt+) and EVT-differentiated (Wnt-) hTSC-derived organoids following 10 days of culture. Bar = 400 μm.
(B) Flow cytometry plots showing cell frequencies of HLA-G, CD49e, and HLA-ABC positive cells in regenerative (Wnt+) and EVT-differentiated hTSC-derived (CT27) organoids.
(C) Relative measurement of mRNA levels by qPCR in EVT-differentiated hTSC-derived organoids (CT27, CT29, CT30) over 21 days (D) of culture. Shown are CTB/progenitor (*TEAD4, ITGA6*), syncytial (*CGB, CSH1*), immature EVT (*ITGA5, NOTCH1*), and mature EVT (*NOTCH2, HLA-G*) genes.
(D) UMAP and gene heatmap plots of combined CT27, CT29, and CT30 single cell hTSCs following culture in regenerative (Wnt+) and EVT-differentiated (Wnt-) conditions after 7 days in culture. UMAP plots are overlain with projected RNA velocity (scVelo) vector field, demonstrating 7 distinct trophoblast clusters representing 3 states (CTB1, CTB2, CTB3, bipotent cCTB, EVT1, EVT2, SCTp). Heatmap shows the average expression of trophoblast- and proliferation-associated genes in each cell state.
(E) UMAP and gene heatmap plots derived from individual hTSC lines (CT27, 2259 cells; CT29, 1446 cells; CT30, 2604 cells) subjected to scRNA-seq analyses. UMAP plots are overlain with projected RNA velocity vector field, demonstrating 5 distinct trophoblast clusters in each hTSC line.
(F) Venn diagram comparing genes shared and distinct between CTB2/CTB3 in chorionic villi and CTB1/CTB2 states in hTSC organoids.
UMAP plots showing expression of BCAM (red) in **(G)** combined (CT27, CT29, CT30) and **(H)** segregated hTSC-derived organoid cells/states.
(G) UMAP plot of all 7 cell states in hTSC-derived organoids (CT27, CT29, CT30) showing *BCAM* expression (red signal).
(H) UMAP plots of cell states of individual hTSC-derived organoids (CT27, CT29, CT30) showing *BCAM* expression (red signal).

Figure 4

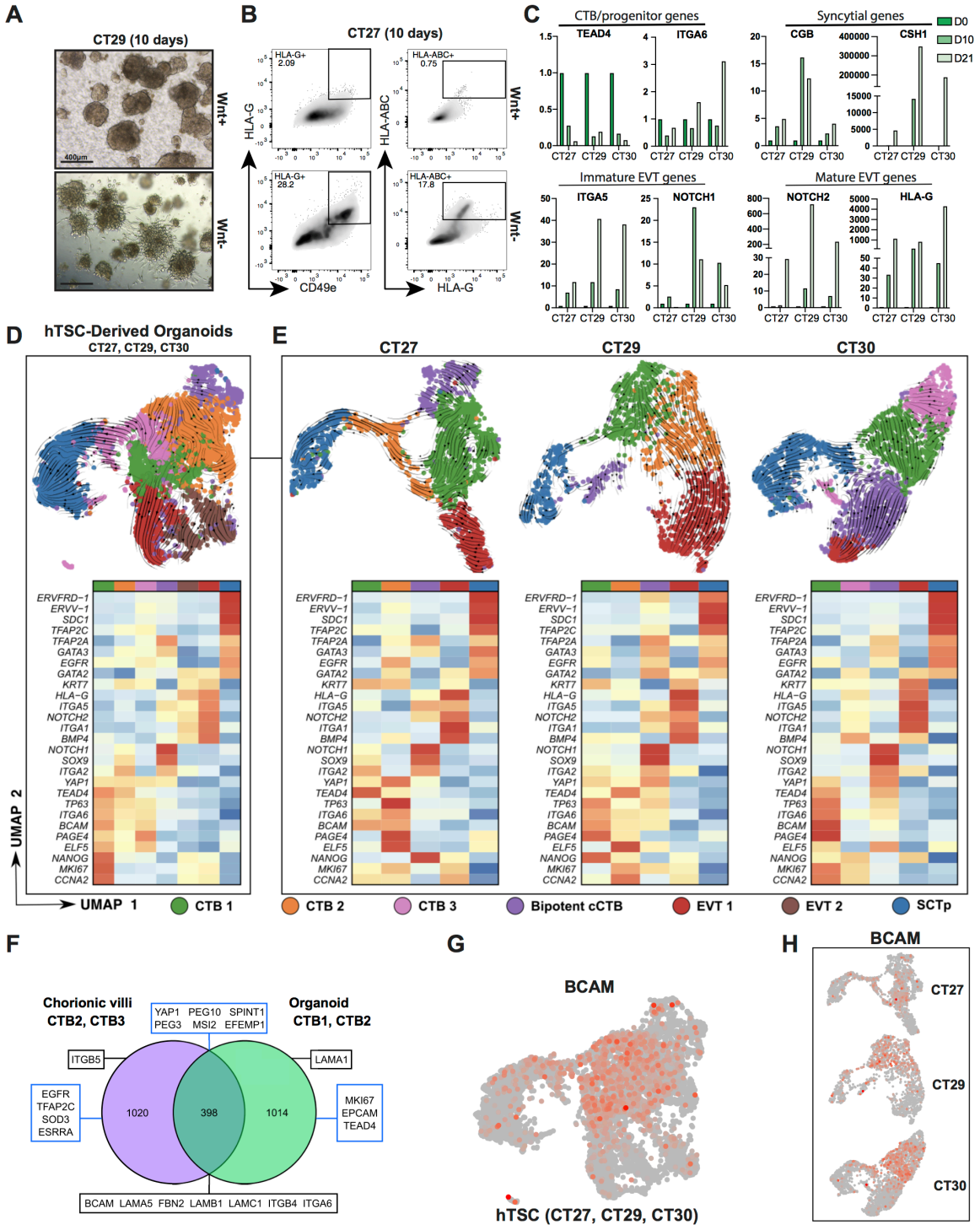
A
CT29 (10 days)
Wnt+
Wnt-
400µm
B
CT27 (10 days)
HLA-G+
2.09
HLA-ABC+
0.75
HLA-G+
28.2
HLA-ABC+
17.8
HLA-G
HLA-ABC
CD49e
HLA-G
C
CTB/progenitor genes
TEAD4
ITGA6
Syncytial genes
CGB
CSH1
D0
D10
D21
Immature EVT genes
ITGA5
NOTCH1
Mature EVT genes
NOTCH2
HLA-G
CT27 CT29 CT30
D
hTSC-Derived Organoids
CT27, CT29, CT30
UMAP 2
UMAP 1
E
CT27
CT29
CT30
ERVFRD-1
ERVV-1
SDC1
TFAP2C
TFAP2A
GATA3
EGFR
GATA2
KRT7
HLA-G
ITGA5
NOTCH2
ITGA1
BMP4
NOTCH1
SOX9
ITGA2
YAP1
TEAD4
TP63
ITGA6
BCAM
PAGE4
ELF5
NANOG
MKI67
CCNA2
CTB 1
CTB 2
CTB 3
Bipotent cCTB
EVT 1
EVT 2
SCTp
F
Chorionic villi
CTB2, CTB3
Organoid
CTB1, CTB2
YAP1 PEG10 SPINT1
PEG3 MSI2 EFEMP1
ITGB5
LAMA1
EGFR
TFAP2C
SOD3
ESRRA
1020
398
1014
MKI67
EPCAM
TEAD4
BCAM LAMA5 FBN2 LAMB1 LAMC1 ITGB4 ITGA6
G
BCAM
hTSC (CT27, CT29, CT30)
H
BCAM
CT27
CT29
CT30

973 **Figure 5: BCAM enrichment establishes a regenerative/growth advantage in trophoblast**
974 **organoids**
975
976 **(A)** Immunofluorescence (IF) images of BCAM and keratin-7 (KRT7), human chorionic gonadotrophin
977 (hCG), and HLA-G in early (6.3 weeks) and late (11.2 weeks) first trimester placental villi. Nuclei are
978 stained with DAPI (white). Bars = 100μm.
979 **(B)** IF images of BCAM, hCG and Ki67 in hTSC-derived organoid (CT29) cultured in regenerative
980 (Wnt+) media for 7 days.
981 **(C)** Cell sorting workflow for isolating $BCAM^{hi}$ and $BCAM^{lo}$ EGFR+ CTBs in hTSC (CT29)-derived
982 organoids.
983 **(D)** Bright field images of hTSC (CT29) $BCAM^{hi}$ and $BCAM^{lo}$ –derived organoids cultured over 11
984 days in regenerative Wnt+ media. Bars = 200μm.
985 **(E)** Colony area (μm^2) of $BCAM^{hi}$ and $BCAM^{lo}$ hTSC (CT29)-derived organoids cultured over 11 days
986 (D).
987 **(F)** Flow cytometric panels showing expression of BCAM and EGFR in $BCAM^{hi}$ and $BCAM^{lo}$, CT29-
988 derived organoids following 11 days of culture.
989 **(G)** Heatmap showing levels of select differentially expressed genes from CTB expressing high (hi) or
990 low (lo) levels of *BCAM* in the CTB1 state of CT29-derived organoids following 7 days of culture.

Figure 5

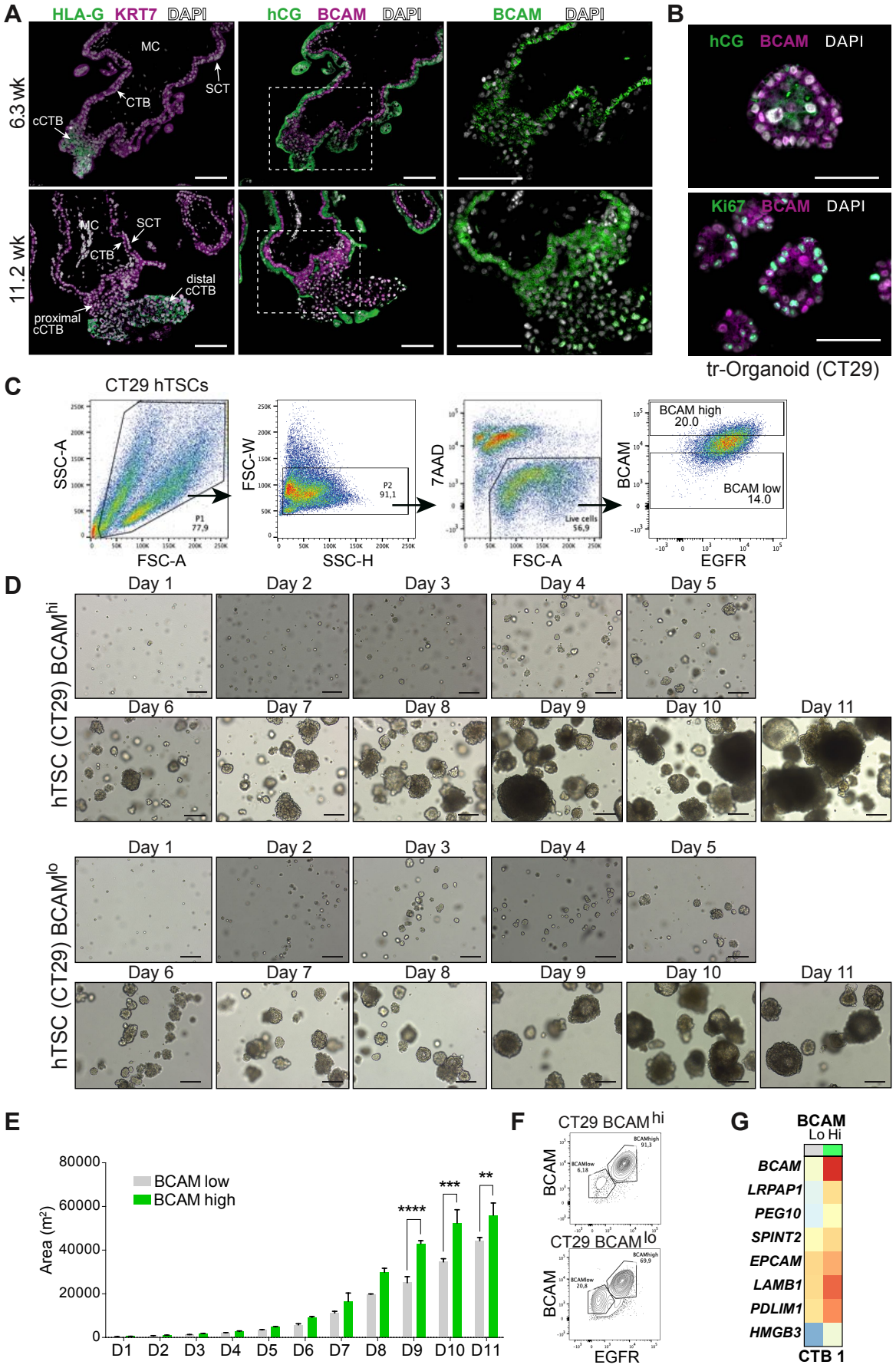
A
HLA-G KRT7 DAPI
hCG BCAM DAPI
BCAM DAPI
6.3 wk
11.2 wk
MC
SCT
CTB
cCTB
distal cCTB
proximal cCTB
B
hCG BCAM DAPI
Ki67 BCAM DAPI
tr-Organoid (CT29)
C
CT29 hTSCs
SSC-A
FSC-A
P1 77,9
FSC-W
SSC-H
P2 91,1
7AAD
FSC-A
Live cells 56,9
BCAM
EGFR
BCAM high 20.0
BCAM low 14.0
D
hTSC (CT29) BCAM hi
hTSC (CT29) BCAM lo
Day 1
Day 2
Day 3
Day 4
Day 5
Day 6
Day 7
Day 8
Day 9
Day 10
Day 11
E
Area (m²)
BCAM low
BCAM high
D1 D2 D3 D4 D5 D6 D7 D8 D9 D10 D11
****
***
**
F
CT29 BCAM hi
CT29 BCAM lo
BCAM
EGFR
G
BCAM
Lo Hi
BCAM
LRPAP1
PEG10
SPINT2
EPCAM
LAMB1
PDLIM1
HMGB3
CTB 1

991 **Supplemental Figure 1: Sample quality control and single cell characterization of the first**
992 **trimester human maternal-fetal interface**
993
994 **(A – C)** Violin plots showing the distribution of the raw number of features **(A)**, the raw number of
995 counts **(B)**, and the percent mitochondrial DNA content remaining post quality control and data pre-
996 processing **(C)** captured per cell during sequencing for each sample. Samples 1-6 (teal) represent the
997 placental tissue samples sequenced by the Beristain lab, samples 7-11 (red) represent the placental
998 tissue samples acquired from ArrayExpress, and samples 12-15 (grey) represent the decidual tissue
999 samples acquired from ArrayExpress.
1000 **(D)** Scatter plot showing the distribution of captured cells across principal components 1 and 2
1001 following dimensional reduction in principal component space. Cell positions are calculated based on
1002 cell embeddings calculated during dimensional reduction by principal component analysis. Cells are
1003 colour coordinated by source with teal representing those cells originating from placental tissue
1004 samples sequenced by the Beristain lab and red representing those cells originating from placental and
1005 decidual tissue samples acquired from ArrayExpress.
1006 **(E)** UMAP plot of 50,790 captured cells, demonstrating 31 distinct clusters identified within the first
1007 trimester human maternal fetal interface. Dashed lines separate maternal decidual immune cells from
1008 non-immune cells and fetal placental trophoblasts. Cells are colour coordinated by identity and
1009 abbreviations are identical to those in Figure 1A. Epigland: epiglandular cell, fetal Endo: fetal
1010 endothelial cell, dEndo: decidual endothelial cell, dSC: decidual stromal cell PV: perivascular cell,
1011 pFib: placental fibroblast, Hb: fetal Hofbauer cell, M1: macrophage cell 1, M2: macrophage cell 2,
1012 uNK: uterine natural killer cell.
1013 **(F)** UMAP projection of the captured maternal fetal interface cells, stratified by gestational age. Early
1014 (left panel): 9803 early first trimester cells from each identified cluster captured between 6-7 weeks
1015 gestational age, before the onset of maternal placental vascularization. Late (right panel): 40,987 late
1016 first trimester cells from each identified cluster captured between 9-12 weeks gestational age, after the
1017 onset of maternal placental vascularization. Cell cluster names and colours correspond to those in
1018 Supplemental Figure 1E.
1019 **(G)** Heatmap showing the average expression of known immune, non-immune, and trophoblast gene
1020 markers, as well as proliferation gene markers in each identified cluster. Cell cluster names and colours
1021 correspond to those in Supplemental Figure 1E.
1022 **(H)** Stacked bar plot showing the percent distribution of cells in each cluster with gene signatures
1023 representing a cell in the gap 1 phase of proliferation, the gap 2 or mitotic phases of proliferation, or the
1024 synthesis phase of proliferation. Cell cluster names and colours correspond to those in Supplemental
1025 Figure 1E and abbreviations are identical to those in Figure 1F.
1026 **(I)** UMAP plots showing gene expression in red of a mesenchymal cell gene marker (*VIM*), an immune
1027 cell gene marker (*PTPRC*, encoding the CD45 protein), endothelial cell gene markers (*CD34* and
1028 *VCAM1*), and a fibroblast gene marker (*ACTA2*).
1029 **(J)** UMAP plots showing gene expression in red of known trophoblast gene markers used to subset and
1030 purify first trimester human trophoblasts from other cells within the maternal fetal interface.
1031

1032

1033 **Supplemental Figure 2: Branched pseudotime ordering aligns key gene pathways to the villous**
1034 **and extravillous differentiation trajectories**
1035
1036 **(A)** Pseudotime trajectory plot showing trophoblasts ordered along the branched trajectory. Cells are
1037 colour coordinated by pseudotime value, with pseudotime increasing as cells move away from the root
1038 along the trajectory.
1039 **(B)** Cells are colour coordinated by cluster identity, with progress towards SCT indicated with a dashed
1040 arrow and progress towards EVT indicated with a solid arrow, moving away from the indicated
1041 trajectory root. Cell cluster names and colours correspond to those in Figure 1C.
1042 **(C-D)** Branched pseudotime heatmap showing relative gene expression changes and average cluster
1043 gene expression levels, respectively, of genes involved in the WNT signaling pathway, the HIPPO
1044 signaling pathway, the NOTCH signaling pathway, and the EGFR signaling pathway.
1045
1046
1047 **Supplemental Figure 3: Monocle3 pseudotime quantification supports identification of CTB2 as**
1048 **the progenitor origin**
1049
1050 **(A)** UMAP plot with constructed trajectory graph overlain. Cells are colour coordinated by relative
1051 pseudotime value.
1052 **(B)** UMAP plot with constructed trajectory graph overlain. Cells are colour coordinated by cluster
1053 identity. Cell cluster names and colours correspond to those in Figure 1C.
1054 **(C)** UMAP plot highlighting the constructed trajectory graph which describes the path taken as CTB
1055 state 2 progresses into CTB state 3. Cells are colour coordinated by cluster. Cluster names and colours
1056 correspond to those in Figure 1C.
1057
1058 **Supplemental Figure 4: Organoid colonies in BCAM^{hi} and BCAM^{lo} sorted organoids**
1059 Bar graph shows the average of numbers of organoid colonies from BCAM^{hi} and BCAM^{lo} –sorted
1060 CT29 organoids cultured over 11 days. Grey bars = BCAM^{lo}; Green bars = BCAM^{hi}.

Supplemental Figure 1

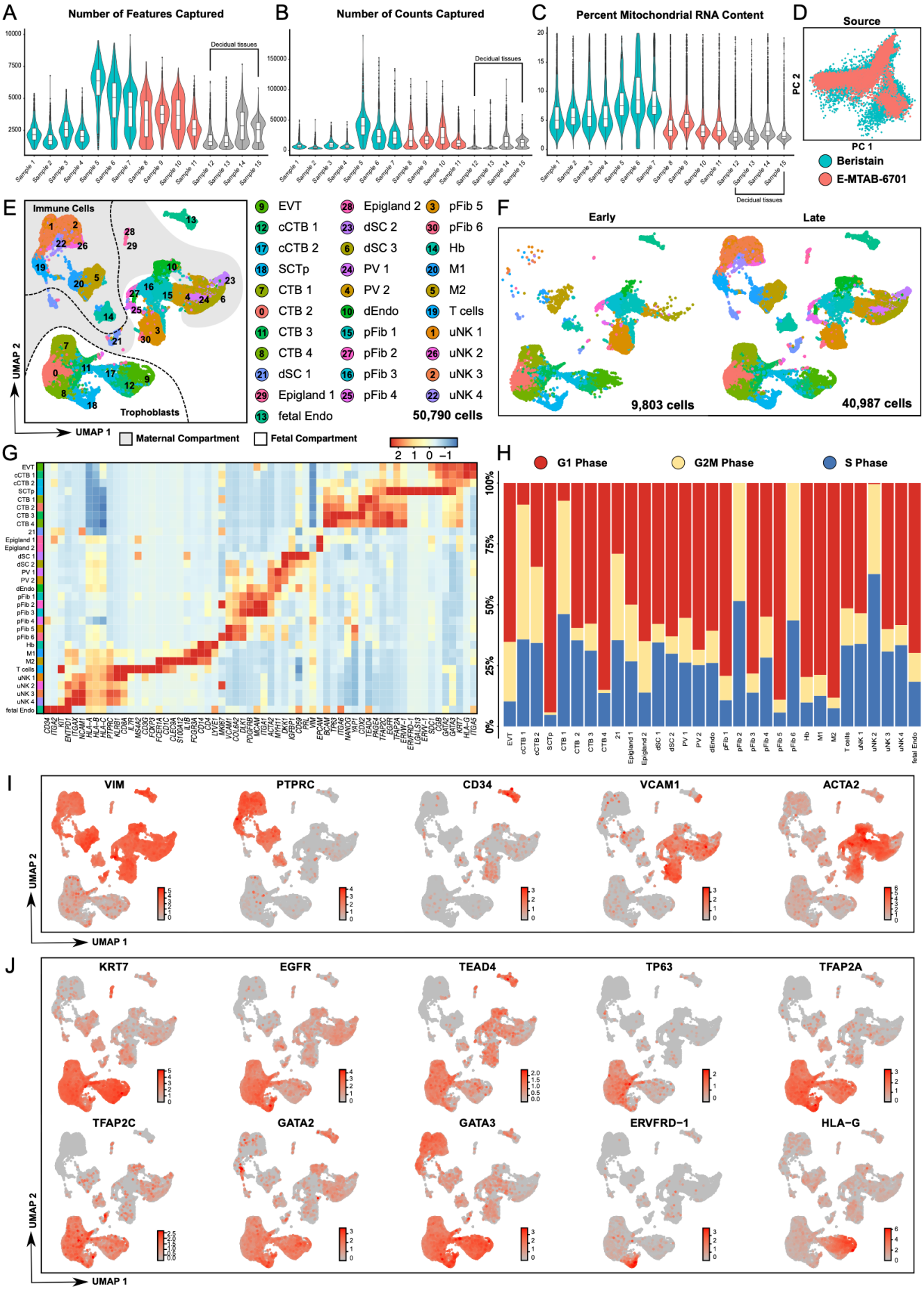

Supplemental Figure 2

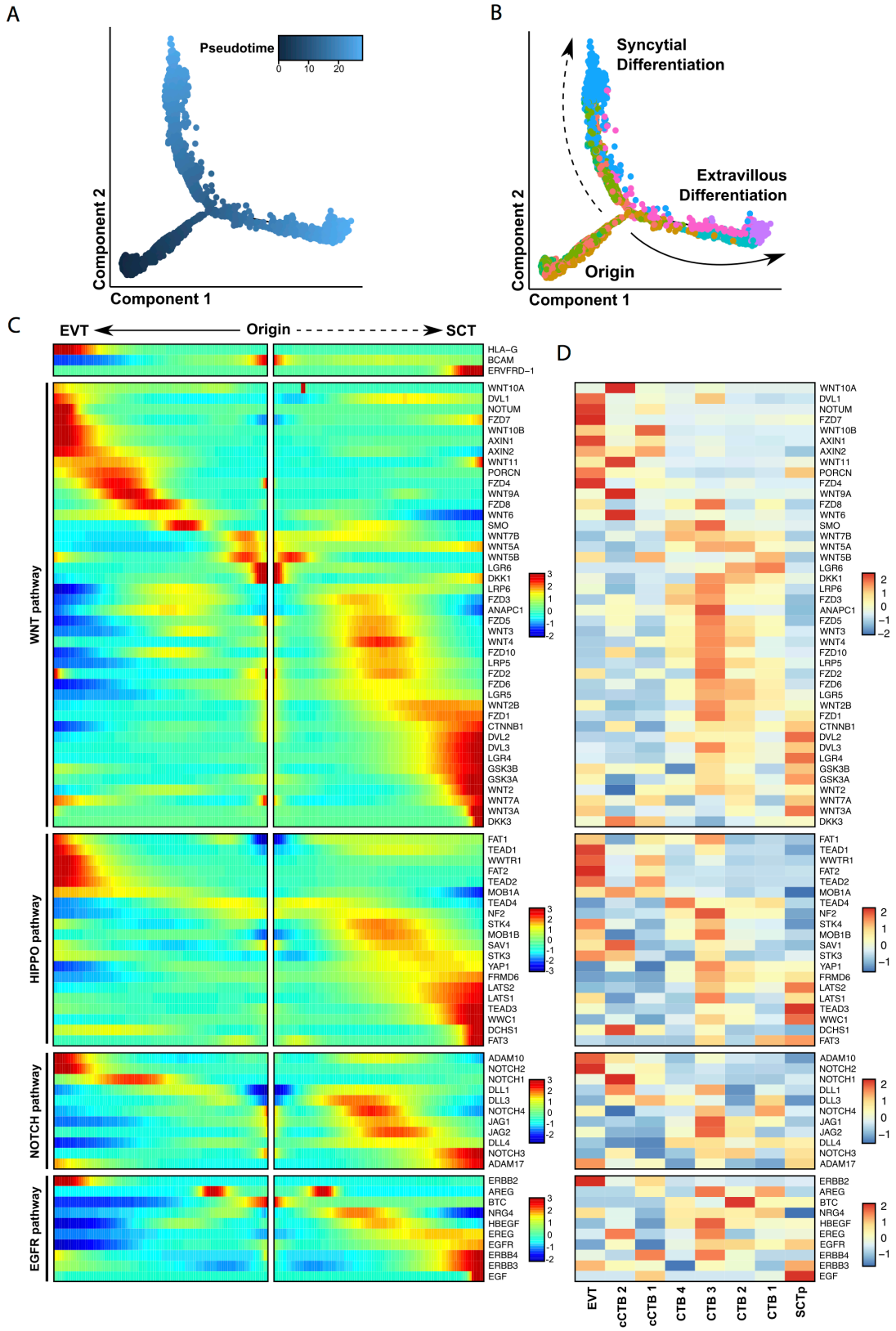

Supplemental Figure 3

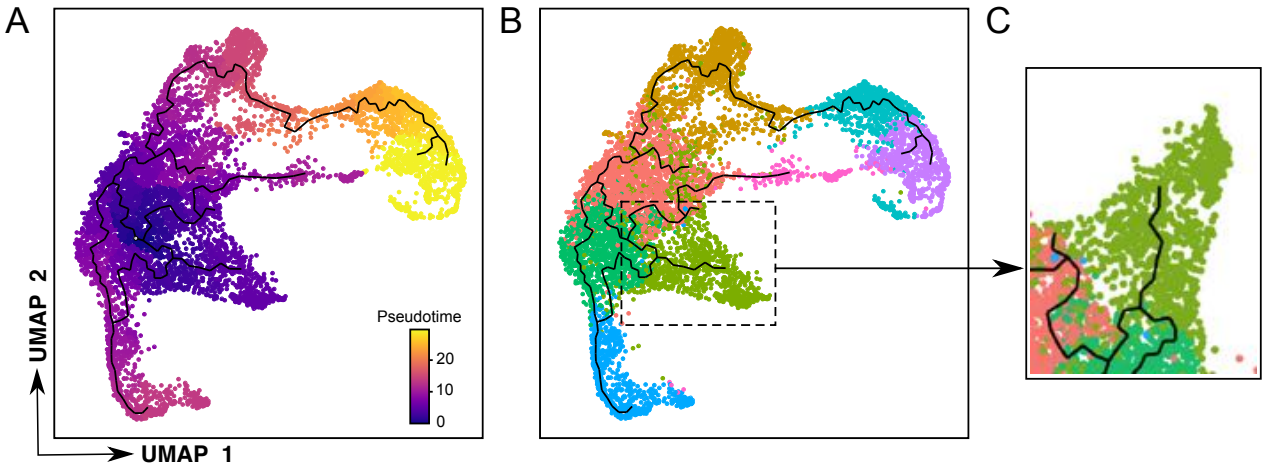
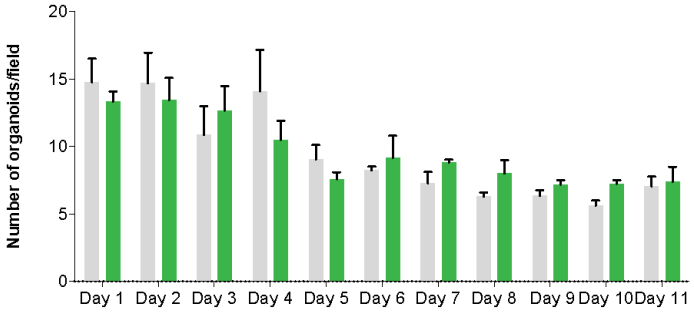
Supplemental Figure 4